
Research Articles: Development/Plasticity/Repair

Slow waves promote sleep-dependent plasticity and functional recovery after stroke

<https://doi.org/10.1523/JNEUROSCI.0373-20.2020>

Cite as: J. Neurosci 2020; 10.1523/JNEUROSCI.0373-20.2020

Received: 10 February 2020

Revised: 15 September 2020

Accepted: 24 September 2020

This Early Release article has been peer-reviewed and accepted, but has not been through the composition and copyediting processes. The final version may differ slightly in style or formatting and will contain links to any extended data.

Alerts: Sign up at www.jneurosci.org/alerts to receive customized email alerts when the fully formatted version of this article is published.

Copyright © 2020 Facchin et al.

This is an open-access article distributed under the terms of the Creative Commons Attribution 4.0 International license, which permits unrestricted use, distribution and reproduction in any medium provided that the original work is properly attributed.

TITLE PAGE

Title: Slow waves promote sleep-dependent plasticity and functional recovery after stroke

Running title: Slow waves promote functional stroke recovery

Authors and affiliations: Laura Facchin¹, Cornelia Schöne¹, Armand Mensen², Mojtaba Bandarabadi¹, Federica Pilotto^{1, 3}, Smita Saxena^{1, 3}, Paul Antoine Libourel⁴, Claudio L.A. Bassetti^{1, 2#}, Antoine R. Adamantidis^{1,2,3#*}

¹Centre for Experimental Neurology, Department of Neurology, Inselspital University Hospital, University of Bern, 3010 Bern, Switzerland.

²Department of Neurology, Inselspital University Hospital, University of Bern, 3010 Bern, Switzerland.

³Department of Biomedical Research, University of Bern, 3010 Bern, Switzerland.

⁴Centre de Recherche en Neurosciences de Lyon, University of Lyon, 69500 Bron, France.

equal contributions.

* correspondence should be addressed to:

Antoine Adamantidis, Department of Neurology, Inselspital University Hospital, University of Bern, Freiburgstrasse 18, 3010 Bern, Switzerland. e-mail: antoine.adamantidis.unibe.ch.

Claudio L.A. Bassetti, Department of Neurology, Inselspital University Hospital, University of Bern, Freiburgstrasse 18, 3010 Bern, Switzerland. e-mail: claudio.bassetti@insel.ch.

Number of pages: 45

Number of figures: 8

Number of words for:

abstract: 250

introduction: 493

discussion: 1474

Conflict of interest: The authors declare no competing financial interest.

Acknowledgment: We thank all members of the Adamantidis and Bassetti Labs and the technical assistance of Andrea Oberli and Joel Gyger. LF was supported by the Inselspital University Hospital of Bern and the SNF Sinergia (CRSII3_160803) grant. AA was supported by the Human Frontier Science Program (RGY0076/2012), Inselspital University Hospital of Bern, Swiss National Science Foundation (31003A_156156), European Research Council (725850), Sinergia (CRSII3_160803), the University of Bern and the Bern University Hospital.

Authors contribution: LF, FP, SS, CB and AA designed the research; LF and CS performed the research; LF, CS, AM, MB analyzed the data; PAL developed the sleep scoring system. All authors wrote the paper.

48 **ABSTRACT**

49 Functional recovery after stroke is associated with a remapping of neural circuits. This
50 reorganization is often associated with low frequency high amplitude oscillations in the peri-
51 infarct zone in both rodents and humans. These oscillations are reminiscent of sleep slow
52 waves (SW) and suggestive of a role for sleep in brain plasticity that occur during stroke
53 recovery, however, direct evidence is missing. Using a stroke model in male mice, we
54 showed that stroke was followed by a transient increase in NREM sleep accompanied by
55 reduced amplitude and slope of ipsilateral NREM sleep SW. We next used 5 ms optical
56 activation of Channelrhodopsin 2-expressing pyramidal neurons, or 200 ms silencing of
57 Archaelorhodopsin T-expressing pyramidal neurons, to generate local cortical UP, or DOWN,
58 states, respectively, both sharing similarities with spontaneous NREM SW in freely-moving
59 mice. Importantly, we found that single optogenetically-evoked SW (SW^{opto}) in the peri-
60 infarct zone, randomly distributed during sleep, significantly improved fine motor
61 movements of the limb corresponding to the sensorimotor stroke lesion site, as compared to
62 spontaneous recovery and control conditions, while motor strength remained unchanged. In
63 contrast, SW^{opto} during wakefulness had no effect. Furthermore, chronic SW^{opto} during sleep
64 were associated with local axonal sprouting as revealed by the increase of anatomical pre-
65 and post-synaptic markers in the peri-infarct zone and corresponding contra-lesional areas to
66 cortical circuit reorganization during stroke recovery. These results support a role for sleep
67 SW in cortical circuit plasticity and sensorimotor recovery after stroke and provide a
68 clinically-relevant framework for rehabilitation strategies using neuromodulation during
69 sleep.

70

71

72 **SIGNIFICANCE STATEMENT**

73 Brain stroke is one of the leading causes of death and major disabilities in elderly worldwide.
74 A better understanding of the pathophysiological mechanisms underlying spontaneous brain
75 plasticity after stroke, together with an optimization of rehabilitative strategies, are essential
76 to improve stroke treatments. Here, we investigate the role of optogenetically-induced sleep
77 slow waves in an animal model of ischemic stroke and identify sleep as a window for post-
78 stroke intervention that promotes neuroplasticity and facilitates sensorimotor recovery.

79

80 INTRODUCTION

81 Stroke is an acute brain injury caused by a sudden decrease in cerebral blood flow, followed
82 by local inflammation (Huang et al., 2006), excitotoxicity (Lai et al., 2014) and cell death
83 (Small et al., 1999). Changes in neuronal excitability after stroke are thought to promote
84 long-term plasticity in surviving neurons that contributes to the reorganization of cortical
85 maps and to the underlying level of axonal sprouting supporting brain functions (Carmichael,
86 2012; van Meer et al., 2012; Silasi and Murphy, 2014), as observed in rodents (Nudo, 1997;
87 Murphy and Corbett, 2009; Carmichael et al., 2017) and humans (Khedr et al., 2005;
88 Lindenberg et al., 2010). To date, pharmacological treatments and non-invasive brain
89 neuromodulation techniques hold promise in improving plasticity and functional recovery
90 both in animal model (Zhang et al., 2007; Yoon et al., 2012) and human (Robinson et al.,
91 2008; Ameli et al., 2009; Talelli et al., 2012), yet the underlying mechanisms remain unclear.

92
93 Post-stroke hyperexcitability of surviving neurons contributes to the transient low-frequency
94 (~ 1 Hz, 200-500 ms in duration), high amplitude, rhythmic waves (also coined ‘bistable
95 state’) originating in the peri-infarct zone and propagating to contra-lesional brain areas. This
96 distinctive 1-Hz slow and synchronous neural activity in the peri-infarct zone shares
97 similarities with slow waves (SW) typically recorded during non-rapid eye movement
98 (NREM) sleep in rodents and human. Indeed, SW reflect bistable states of thalamocortical
99 neuron populations, described as a switch between UP states where depolarised membrane
100 potentials are accompanied by high spiking activity, and DOWN states during which cells are
101 hyperpolarized and show low spiking activities in cats (Steriade et al., 1993), rodents
102 (Vyazovskiy et al., 2009; Zucca et al., 2017), non-human primates (Xu et al., 2019) and
103 human (Cserscsa et al., 2010). These SW were hypothesized to guide axonal sprouting and

circuit rewiring through the formation of new connections after brain lesions (Carmichael and Chesselet, 2002) facilitating recovery, however this has not been directly demonstrated.

Extensive experimental evidence suggests a fundamental role for intact sleep, and SW in particular, in enhancing brain plasticity during spontaneous sleep (Tononi and Cirelli, 2016; Timofeev and Chauvette, 2017) and stroke recovery (Duss et al., 2017). The detrimental effects of sleep disturbances (Kaneko et al., 2003; Baglioni et al., 2016) and the beneficial effect of pharmacological NREM sleep enhancement after stroke support the hypothesis that SW contribute to brain plasticity underlying post-stroke functional and cognitive recovery both in animal models (Gao et al., 2008; Hodor et al., 2014) and patients (Vock et al., 2002; Siccoli et al., 2008; Sarasso et al., 2014).

Here, we used an optogenetic approach inspired by global and local SW changes after stroke to rescue SW-like activity in freely-moving mice. Optogenetic activation of pyramidal neurons in the peri-infarct zone during NREM sleep improved fine motor movements as compared to experimental control conditions. In contrast, optogenetically-evoked SW (SW^{opto}) during wakefulness had no effect. Importantly, SW^{opto} evoked recovery after stroke was associated with axonal sprouting in the peri-infarct zone and corresponding contra-lesional areas.

MATERIALS AND METHODS

Animals

C57BL/6JRj male mice (https://www.janvier-labs.com/en/fiche_produit/c57bl-6jtrj_mouse/) (5-6 weeks old, 23-30 grams) were used in the study. Animals were individually housed in

129 custom-designed polycarbonate cages (300 mm x 170 mm) under controlled conditions
 130 (regular circadian cycle of 12:12 h light:dark; light on at either 4 a.m. or 8 p.m. according to
 131 experimental design; constant temperature 22 ± 1 °C and humidity 30-50%). Throughout the
 132 experiment animals were freely-moving with *ad libitum* food and water. Animals were kept
 133 in groups of 2-5 per IVC cage before instrumentation and after viral injection surgery.
 134 Following implantation mice were all housed individually. Animals were tethered, allowed to
 135 adapt to the EEG/EMG and optic stimulation cables in their home cage for at least 5-7 days,
 136 and remained plugged for the duration of the experiment. Animals were detached from all
 137 tethers for 4 days following stroke or sham surgery and for the duration of behavioural
 138 testing. Animals were randomly assigned to eight experimental groups: Channelrhodopsin
 139 (ChR2) transfected animals subjected to stroke (ChR2^{stroke}), ChR2 transfected animals
 140 subjected to stroke and optogenetically stimulated mainly during wakefulness
 141 (ChR2^{stroke_wake}), Archaelrhodopsin (ArchT) transfected animals subjected to stroke
 142 (ArchT^{stroke}), mCherry transfected animals subjected to stroke (mCherry^{stroke}), mCherry
 143 transfected animals subjected to sham surgery (mCherry^{sham}), Naive, Sham and Stroke.
 144 Animals that displayed baseline asymmetry in limb usage or did not show a drop in cerebral
 145 blood flow (CBF) by ~ 80% during middle cerebral artery occlusion (MCAo) surgery were
 146 excluded from further experimental tests. Viral injections were performed when animals were
 147 5-6 weeks of age, instrumentation at 8 weeks of age and stroke/ sham surgery at 10 weeks of
 148 age. Between surgeries and before being tethered, animals were let recover undisturbed for at
 149 least 7 days. Naive mice did not undergo any surgical procedures. An additional set of
 150 heterozygous Tg(VGAT-Cre) mice, (5-6 weeks old, 23-30 grams) was used for an
 151 optogenetic screening of slow waves-like oscillations inducing protocols. All animals were
 152 treated according to animal care laws and experimental procedures were approved by local

153 authorities (Veterinary Office, Canton of Bern, Switzerland; licence numbers BE 113/13 and
154 BE 41/17).

155

156 **Viral targeting**

157 For a detailed description of the surgical procedure refer to Herrera et al., 2016. Briefly, 5-6
158 weeks old animals were anesthetized with isoflurane (4.0% induction; 1.0-1.5%
159 maintenance). Body temperature was constantly monitored and kept at physiological range
160 using a rectal thermoprobe and feedback-controlled heating system. Animals were fixed in a
161 digital stereotaxic frame and analgesia was administered subcutaneously (Meloxicam,
162 5mg/kg). Animals were randomly assigned to receive 0.6 μ L of recombinant AAV carrying
163 either CaMKII-hChR2 (H134)-EYFP (activation), CaMKIIa-eArchT3.0-EYFP (silencing) or
164 CaMKIIa-mCherry (control) respectively. Plasmids were stereotactically injected (0.1
165 μ L/min infusion rate) through a 28 G needle (Plastic One), connected by a tubing to a 10 μ L
166 Hamilton syringe in an infusion pump (Model 1200, Harvard Apparatus). Injections were
167 performed within the left (prospective ipsilateral) primary somatosensory forelimb cortex
168 (iS1FL, AP: -0.10 mm; ML: -2.00 mm; DV: -0.7 mm). Animals were given 7 days of
169 recovery prior to instrumentation surgery. Tg(VGAT:Cre) mice underwent identical surgical
170 procedures as wild type animals, randomly assigned to receive 0.6 μ L of recombinant AVV
171 carrying Ef1 α -DIO-ChR2-EYFP (activation), Ef1 α -DIO-ArchT-EYFP (silencing) or Ef1 α -
172 DIO-EYFP (control) respectively. All plasmids were obtained from the University of North
173 Carolina Vector Core Facility. Mice belonging to Sham, Stroke and Naive groups did not
174 received any AAV injection.

175

176 **Instrumentation**

177 Animals were chronically implanted with a unilateral optic fiber (200 μ m in diameter) within
 178 the iS1FL (AP: -0.10 mm; ML: -2.00 mm; DV: -0.5 mm) and an electroencephalography
 179 (EEG)/electromyography (EMG) connector. As previously reported (Gent et al., 2018),
 180 animals received analgesia (Meloxicam, 5mg/kg), were anaesthetised with isoflurane and
 181 anchored to a stereotaxic frame. Five stainless steel EEG electrode screws were inserted
 182 through each animal's skull; two screws over the frontal cortices (AP: +2 mm; ML: \pm 2mm),
 183 two screws over the posterior cortices (AP: -4 mm; ML: \pm 2 mm) and one screw over the
 184 olfactory bulb as ground. For the stimulation recordings, the EEG signals from the frontal and
 185 posterior channels were referenced to each other directly, leaving only two EEG traces, one
 186 per hemisphere. Finally, two bare-ended EMG wires were sutured to the neck muscles to
 187 record postural tone. A subset of animals was additionally implanted with four tetrodes to
 188 record local field potentials (LFPs) and single unit activity during optogenetic stimulation, as
 189 well as EEG/EMG signals. Tetrodes were constructed by twisting four tungsten wires
 190 together (10 μ m in diameter, CFW0010954, California Fine Wire) and briefly heating them
 191 to favour the bond coating of each wire to another. Tetrodes were lowered within the iS1FL
 192 (AP: -0.10 mm; ML: -2.00 mm; DV: -0.5 mm), the ipsilateral primary motor cortex (iM1,
 193 AP: +1.10 mm; ML: -1.5 mm; DV: -1.20 mm), the contralateral S1FL (cS1FL, AP: -0.10
 194 mm; ML: +2.00 mm; DV: -0.5 mm) and the contralateral M1 (cM1, AP: +1.10 mm; ML:
 195 +1.5 mm; DV: -1.20 mm) respectively. The tetrode positioned in iS1FL was glued to the
 196 optic fiber, where the tip of the tetrode extended for ~0.2 mm beyond the end of the fiber
 197 (optrode). Optic fibers and implants were permanently secured to the skull with C&B
 198 Metabond (Patterson Dental) and methacrylate cement (Paladur). Animals were monitored
 199 post-operatively and left to recover undisturbed for at least 7 days. Animals were then
 200 plugged to the EEG/EMG/optic stimulation and tetrodes tethers (Neuralynx headstage).
 201 Black nail polish was applied at the connection point between optic fiber and patch cord to

202 limit laser light spreading during optogenetic stimulations. The implantation procedure for
 203 animals belonging to Sham and Stroke groups did not include either optic fiber or tetrodes
 204 placement.

205

206 **Transient focal cerebral ischemic stroke**

207 Mice underwent MCAo via intraluminal filament model (Doeppner et al., 2010) at around 10
 208 weeks of age. To begin, mice were anaesthetised with isoflurane as previously described and
 209 placed in a prone position. Physiological temperature was maintained as mentioned above.
 210 The left common carotid artery (CCA) was dissected from the surrounding connective tissue.
 211 A monofilament suture (7-0 silicon rubber coated, coating length 5-6 mm, Doccol
 212 Corporation) was inserted in the CCA and introduced into the lumen of the MCA. The
 213 monofilament was left in place for 45 min to induce both striatal and cortical infarct and
 214 consequently withdrawn to allow the reperfusion of the territory targeted by the MCA. CBF
 215 was constantly monitored by a Laser Doppler probe (Moor Instrument, VMS-LDF2) glued to
 216 the skull above the MCA region. Ischemic stroke induction was considered successful when
 217 the CBF showed a ~ 80 % reduction from baseline values, as well as reperfusion of the MCA
 218 territory. Following surgery, mice were daily checked for pain and weight loss, received
 219 mashed, watered food, subcutaneous analgesia and 0.9% saline. Animals belonging to the
 220 Naive group did not undergo stroke or sham surgery. No filament was inserted into the MCA
 221 during sham surgery. Following MCAo, 40% of animals assigned to the Stroke group and
 222 33% of all animals allocated to optogenetic stimulations did not survive the post-operation
 223 phase.

224

225 **Optogenetic stimulation**

Lasers (Laserglow Technologies) attached to the unilateral fiber via patch cord (Thorlabs) were triggered through TTL with a pulse stimulator (Master - 9, AMPI), this latter controlled by a function generator (Agilent, 33220A 20MHz Function/ Arbitrary Waveform Generator) to induce random pulse sequences. Animals received daily 2 h of randomly distributed single laser light pulses (inter-pulses interval 3-30 sec), from post-stroke day 5 until day 15. The random distribution of light pulses was selected to avoid hypersynchrony and entrainment of oscillatory activities which, *per se*, might influence the observed parameters. The optogenetic stimulation was semi-chronic: light pulses were distributed across sleep and wake states without simultaneous behavioural scoring by the experimenter and consequent state specific stimulation. Indeed, daily and chronic stimulation (11 days) of several animals (experimental and control were run in parallel) is not suited for a single experimenter. The specific time allocated for optogenetic intervention was therefore selected according to the natural distribution of the majority of NREM sleep and wakefulness episodes throughout the 12h light:dark cycle of the animals. Two stimulation protocols were employed: ChR2-expressing animals received 5 ms blue light pulses (473 nm wavelength), ArchT-expressing mice were stimulated with 200 ms green light pulses (532 nm wavelength) and mCherry-expressing animals were randomly subjected to either 200 ms or 5 ms light pulses. To assess whether the effect of SW^{opto} on functional recovery was specific to brain activity occurring during sleep, in a separate group of animals ($ChR2^{stroke_wake}$) optogenetic stimulations were also delivered during the first part of the dark phase, when animals were mostly awake. Based on pre-instrumentation testing of both optic fiber and patch cord outputs, light power was set at 20-25 mW.

Data acquisition

250 EEG and EMG signals were amplified (Model 3500, AM System) and digitized at 512 Hz
 251 (NIDAQ 6363, National Instruments) using a sleep recording software (MATLAB written
 252 software, DaqReverse). A 24 h baseline of spontaneous sleep-wake behaviour was recorded
 253 for all animals. Stroke and Sham animals were recorded for 24 h at post-surgery days 1, 3, 5
 254 and 10. All optogenetic stimulations took place between 9 a.m. and 2 p.m., with light on at 4
 255 a.m. for ChR2^{stroke}, ArchT^{stroke}, mCherry^{stroke} and mCherry^{sham}. Since ChR2^{stroke} and
 256 ArchT^{stroke} animals showed similar functional outcomes upon neuronal manipulation during
 257 sleep, an additional ChR2-transfected set of animals received SW^{opto} during animals' active
 258 phase (between 9 a.m. and 2 p.m., lights on at 8 p.m, ChR2^{stroke_wake}), from post-stroke day 5
 259 until day 15. Animals' spontaneous sleep was recorded for 18 h at post-stroke day 5, 6, 8, 12
 260 and 14 respectively. LFPs and EEG/EMG signals were amplified and digitized at 32 kHz
 261 (Cheetah 5 acquisition software, Neuralynx, [https://neuralynx.com/software/cheetah-5.0-](https://neuralynx.com/software/cheetah-5.0-legacy)
 262 legacy).

264 Behavioural tests

265 All animals were trained in four behavioural tests and engaged in daily training sessions for
 266 three consecutive days. Behavioural baselines were acquired prior to stroke/ sham surgery.
 267 Functional outcomes were verified at post-stroke days 4, 7, 10 and 15. All behavioural tests
 268 were conducted at least 3 h apart from optogenetic stimulations and during animals' active
 269 phase (between 5 p.m. and 8 p.m.). Test sessions were recorded with a picamera (Raspberry
 270 Pi) and scored in slow motion (VideoPad software,
 271 <https://www.nchsoftware.com/videopad/index.html>).

272 **Balance beam test:** To assess motor balance and coordination (Brooks and Dunnett, 2009) a
 273 round wooden beam (12 mm in diameter, 80 cm long) was positioned at an angle so that one
 274 end of the beam was 60 cm elevated from the working table. At the beam's elevated end, the

275 animal's home cage served as motivation to complete the task. Soft fabric placed beneath the
 276 beam avoided possible falling injuries. The number of 'paw faults' (forelimb or hindlimb
 277 slipping off the beam) were counted during a maximal testing time of 60 sec. Each animal
 278 underwent three trials per time point and means were calculated.

279 ***Tight rope test***

280 To measure grip strength and endurance (Balkaya et al., 2013) animals were suspended on a
 281 fine rope (60 cm above the working table) between two platforms (80 cm apart from one
 282 another). Mice were positioned at the middle point of the rope exclusively with their
 283 forepaws. The average time needed to reach one of the two platforms was calculated between
 284 two trials. The maximum testing time was 60 sec.

285 ***Corner turn test***

286 To evaluate the presence of unilateral abnormalities (Park et al., 2014) mice were placed in
 287 between two vertical boards forming a 30° angle. Animals left- or right-turn decision was
 288 recorded for a total of 10 trials per testing session. Laterality index was calculated as (number
 289 of left turns – number of right turns)/10.

290 ***Ladder walking rig test***

291 The test was chosen to measure paw accurate placement (Cummings et al., 2007). The
 292 apparatus consisted of a ladder (80 cm long), suspended between two platforms (60 cm above
 293 the working table) with randomly spaced rungs. Paw faults were recorded as animals walked
 294 to reach the home cage at one end of the ladder. Mice performances were scored in slow
 295 motion and the mean of three trials calculated. The position of the rungs was randomly
 296 changed across trials to avoid learning.

297

298 **Signal processing**

299 As previously described (Jego et al., 2013), electrophysiological data were manually scored
 300 in 5 sec epochs and analysed using SlipAnalysis (custom written MATLAB program).
 301 Briefly, three vigilance state were identified based on EEG/EMG frequency and amplitude.
 302 Wakefulness was determined by low amplitude EEG and high activity EMG signals; NREM
 303 sleep as high amplitude and low-frequency EEG (0.5-4 Hz) paired with reduced EMG
 304 activity; REM was characterized by theta rhythm (6-9 Hz) EEG and flat EMG. Microarousals
 305 were defined and scored as cortical fast rhythm and EMG bursts of at least 1 sec. Sleep/
 306 wakefulness scoring was based on the visual characteristics of the contralateral EEG traces
 307 specifically. Electrophysiological analysis was completed using custom MATLAB scripts.

308

309 **Automatic single SW detection**

310 Individual SW were detected during NREM sleep epochs during the first 7 h of the lights ON
 311 period in MATLAB using the SWA-MATLAB toolbox (Mensen et al., 2016), with detection
 312 parameters adjusted to rodents from settings described in Panagiotou et al., 2017. Briefly, in a
 313 first-pass of the data, the negative envelope across the 4 EEG channels was calculated,
 314 filtered between 0.5 and 4 Hz (Chebyshev Type II filter design), and consecutive zero-
 315 crossings were detected. If the duration between successive downward (negative going) zero-
 316 crossing and upward zero-crossing was between 100 msec and 1 sec, then the peak negative
 317 amplitude was examined and was required to be at least 3 deviations from the median
 318 amplitude of all negative peaks in the recording. The amplitude threshold eliminates the
 319 potential individual differences of electrodes reference type, distance to those reference, and
 320 electrode depth that would affect the record amplitude. In a second-pass, the activity over all
 321 4 channels was examined for each slow wave detected on the negative envelope to obtain
 322 individual channel data.

323

324 **Single unit analysis**

325 We performed spike detection and sorting as described previously (Gent et al., 2018). Briefly,
 326 we first extracted multiunit activity from band-pass filtered signals (600-4000 Hz, 4th-order
 327 elliptic filter, 0.1 dB passband ripple, -40 dB stopband attenuation), by applying a detection
 328 threshold of $7.5 \times$ the median of the absolute values of the filtered signal. We then extracted
 329 wavelet coefficients from the detected multiunit activity using a four-level discrete wavelet
 330 transform (Harr wavelet, 'wavedec', MATLAB), and subsequently sorted the coefficients
 331 using the super-paramagnetic clustering. We visually inspected the sorted units and excluded
 332 the clusters with a symmetric shape or an average firing rate less than 0.2 Hz from our
 333 analyses.

335 **Optogenetic response analysis**

336 We assessed the optogenetic response analysis for each vigilance state separately. For unit
 337 activity, we calculated mean firing rates during optogenetic perturbations by averaging firing
 338 rates across trials using a non-overlapping moving window of 5 ms. For LFP analysis, we
 339 averaged raw LFP signals across trials of each vigilance state.

341 **Infarct volume evaluation and immunohistochemistry**

342 Animals were sacrificed at post-stroke day 15 with 15 mg pentobarbital intraperitoneal
 343 injection (Esconarkon ad us. vet., Streuli Pharma) and transcardially perfused with 1x
 344 phosphate buffered saline (PBS) followed by 4% formalin. Brains were post-fixed overnight,
 345 cryoprotected in 30% sucrose (24-48 h at 4°C), frozen in 2-methyl-butane on dry ice and cut
 346 into 40 μ m sections. Every third slice was mounted onto a glass slide, dried at room
 347 temperature (RT), rehydrated and processed for Nissl staining. Briefly, sections were
 348 immersed in Cresyl Violet (Klüver Barrera, Bio-Optica), washed in distilled water and

349 dehydrated in graded alcohols, cleared in Xylene (Sigma-Aldrich) and mounted (Eukitt
 350 mounting medium, Bio-Optica) on microscope slides. Stroke edges were delineated per
 351 section using Imagej software (<https://imagej.nih.gov/ij/>). The damaged area was measured in
 352 each brain slice and multiplied by the distance between brain sections. Stroke volume relative
 353 to the whole brain was calculated as follows: $((\text{volume of contralesional hemisphere} - \text{volume}$
 354 $\text{of ipsilesional hemisphere})/2 * \text{volume of contralesional hemisphere}) * 100$ (Lin et al., 1993).
 355 Fluorescent immunohistochemical staining was performed with free-floating brain sections.
 356 Brain slices were washed in PBS-Triton (PBS-T) and incubated in blocking solution (1 h at
 357 RT; PBS-T with 4% of bovine serum albumin, SIGMA Life Science). Free-floating slices
 358 from Chr2- and ArchT-expressing animals were incubated in a primary antibody to GFP
 359 (chicken IgY fraction anti-GFP, 1:5000, Cat# A10262, RRID:AB_2534023, Life
 360 Technologies) in blocking solution (24-48 h at 4°C). Following repeated washes in PBS-T,
 361 sections were incubated with the secondary antibody (1:500, Cat# ab96947,
 362 RRID:AB_10681017, Abcam) in PBS-T (1 h at RT). Sections were then washed in PBS-T,
 363 mounted and covered on microscope slides.

365 **Axonal sprouting quantification**

366 Four brains per experimental group were randomly chosen for axonal sprouting evaluation.
 367 Brains were fixed, frozen and cut as previously described. Several 40 μm sections per brain
 368 were selected (approximately, from Bregma 1.10 mm to Bregma -0.70 mm) and stained for
 369 Vglut1, PSD-95 and DAPI. Floating sections were washed in PBS and blocked in PBS with
 370 0.5% Triton X-100 and 10% normal donkey serum (NDS, Jakson ImmunoResearch Code:
 371 017-000-121) (2 h at RT). Sections were then incubated with the following primary
 372 antibodies: chicken IgY fraction anti-GFP (Chr2^{stroke} and ArchT^{stroke}, Cat# A10262,
 373 RRID:AB_2534023, Life Technologies), rabbit anti-Vglut1 (Chr2^{stroke}, ArchT^{stroke}, mCherry-

374 expressing animals, 1:1000, Cat# 135 303, RRID:AB_887875, SYSY), goat anti-PSD-95
 375 (ChR2^{stroke}, ArchT^{stroke}, mCherry-expressing animals, 1:500, Cat# ab12093,
 376 RRID:AB_298846, Abcam) and mCherry respectively (mCherry-expressing animals, 1:1000,
 377 Cat# M11217, RRID:AB_2536611, Life Technologies) in PBS containing 3% NDS and
 378 0.5% Triton X-100 solution (overnight at 4°C). Brain slices were repeatedly washed in PBS
 379 and incubated with appropriate secondary antibodies (1:500, Alexa Fluor 488 Ab96947,
 380 Abcam; all others 1:1000, Invitrogen) in PBS containing 3% NDS and 0.5% Triton X-100
 381 solution (2 h at RT). A negative control (no addition of primary antibody) was carried out to
 382 confirm the antibody selectivity. Sections were further stained for DAPI (1:500 in PBS, 10
 383 minutes), washed in PBS, mounted on microscope slides and covered. Photomicrographs
 384 were acquired with Olympus Fluoview 1000-BX61 confocal microscope (Olympus, Tokyo)
 385 fitted with 60X oil-immersion objective (4x zoom, 0.5 μ m step size). Three fields of interest
 386 (52.172 μ m x 52.172 μ m) within iS1FL and cS1FL were imaged in three sections per animal.
 387 Imaris software (Microscopy Image Analysis Software, Bitplane, <https://imaris.oxinst.com/>)
 388 was used to reconstruct the 3D view of the Z stacks and to evaluate pre- and post- synaptic
 389 compartments' density and volume. Briefly, background subtraction, image smoothing via
 390 gaussian filtering and channel intensity adjustment were applied and maintained identical for
 391 all the acquired confocal images. A preliminary stack selection was carried out to localize
 392 puncta distributed within two consecutive stacks. A puncta diameter threshold was specified at
 393 0.6 μ m and when this value was exceeded, puncta were separated upon visual confirmation
 394 by the experimenter.

396 **Statistical analysis**

397 For the analyses of the 24 h recordings of stroke and sham animals, a two-level analysis was
 398 performed using linear mixed models. A first-level analysis on each animal and recording

399 day, including temporal predictors of recording time, time since last wake epoch in order to
400 estimate the homeostatic effect on individual slow wave characteristics across the lights on
401 period as well as the potential differences between the ipsi- and contralateral hemisphere. At
402 the second level, the parameter estimates from the first level data for each animal for each
403 day were used to examine the overall effects of stroke over the course of 10 days after stroke.
404 The potential effects of days, stroke, stimulation group, on sleep parameters and behavioural
405 outcomes were tested using linear mixed models. Sleep and behavioural values from day 0
406 was assigned as a baseline predictor, while those from day 4 were used as pre-stimulation
407 baseline. Main effects and interactions were tested for significance using the log-likelihood
408 ratio test between the full model and the model without the specific factor in question. The
409 effects between the stimulation groups were examined by post-hoc t-tests within the linear
410 mixed model. As an exploratory analysis, macro and micro sleep parameters during the
411 stimulation time were included as a potential predictor of behavioural outcome: percentage of
412 NREM, number of micro-arousals, NREM-to-wake transition ratio, wave incidence, wave
413 amplitude, wave duration, positive and negative slope.

414 For the pre- and post-synaptic markers assessment, statistical comparisons were determined
415 with Student's *t*-test, one-way ANOVA, where corrections for multiple comparisons were
416 carried out using Bonferroni correction, if not otherwise indicated (Prism 6 GraphPad;
417 <https://www.graphpad.com/scientific-software/prism/>). Data are presented as mean \pm standard
418 error of the mean (s.e.m.) and levels of statistical significance were set at threshold $p < 0.05$
419 unless otherwise indicated. Sample sizes were defined based on previous studies (Gao et al.,
420 2008; Jegu et al., 2013; Herrera et al., 2016). For each experiment, sample numbers are
421 indicated in the corresponding figure legends. Animals that did not perform behavioural
422 testing were excluded from the analysis; as well as mice that lost EEG/EMG signals during
423 longitudinal measurements. Data distribution was tested for normality using the Lilliefors test

on the residuals from each linear mixed model calculated and found to be normally distributed. Experiments were not conducted in blinded fashion.

Data availability

Dataset and coding supporting the current study are available from the corresponding author upon request.

RESULTS

Stroke alters sleep architecture and SW profile

SWs-like oscillations are frequently observed in peri-infarct zone during NREM sleep and wakefulness (Yokoyama et al., 1996; Murri et al., 1998; Fernandez-Bouzas et al., 2002). To refine the characterization of brain activity after stroke, including SW features, we first quantified the changes of sleep-wake architecture and sleep quality from animals subjected to MCAo and sham surgeries (Fig. 1A, B). Animals were chronically implanted with EEG/EMG electrodes for longitudinal sleep recordings prior to, and at 1, 3, 5, and 10 days after MCAo (see Methods; Fig. 1C). To control for multiple comparisons between the 8 sleep metrics, the significance threshold was reduced to $p < 0.0063$ (i.e. $0.05/8$; Bonferroni correction). MCAo resulted in an initial increase of NREM sleep duration with group differences dampening over the days recorded (Figure 1E, *Day by Stroke* interaction: $LR(1) = 7.977$, $p = 0.0047$). Significant main effects of stroke were found for total wake duration (Figure 1D; $LR(2) = 22.385$, $p < 0.0001$); and wake bout duration ($LR(2) = 34.502$, $p < 0.0001$), but this general effect was not significantly different over the days after correction (*Day by Stroke* interaction: $LR(1) = 4.328$, $p = 0.0375$). No significant results were observed for REM sleep total duration (Fig. 1F). We further explored the potential effect of stroke size

449 within the MCAo group on all sleep architecture measures but found no main effects or
 450 interaction effects with the day of recording (all p -values > 0.0063).

451 NREM sleep instability, describing the ratio between the animals' capacity of remaining
 452 asleep compared to waking up, showed that stroke animals were significantly more likely to
 453 wake up (Fig. 1J; $LR(2) = 14.918$, $p = 0.0006$).

454 The number of microarousals, scored as single epoch of 1 sec (minimum) increased EMG
 455 signal within a NREM sleep episode, did not differ between Stroke and Sham (Fig. 1K;
 456 $LR(2) = 4.651$, $p = 0.0977$).

457

458 To assess SW features and changes after MCAo stroke, animals were prepared for
 459 simultaneous recordings of EEG/EMG, LFPs or single/ multi-units activities in iS1FL,
 460 cS1FL, iM1 and cM1 layer V (see Methods and Fig. 2B for illustration). Clear periods of
 461 neuronal quiescence corresponding to cortical DOWN states confirmed the selectivity of our
 462 SW detection method (see Methods for detection criteria; Fig. 2A-D). Indeed, perilesional
 463 tetrodes recordings of unit activity in S1FL showed suppression, and subsequent increase, in
 464 neuronal activity (Fig. 2D, top), validating the average unit firing rate observed during the
 465 detected SW (Fig. 2D, bottom). Both local and global SW occurred across all recorded
 466 neocortical areas (Fig. 2A), consistent with previous reports in rodents and humans (Huber et
 467 al., 2004; Vyazovskiy et al., 2011). If individual waves are detected across the 24 h period,
 468 we observed a significant reduction of ipsilateral SW's amplitude by $-13.2 \pm 7.3\%$ after
 469 stroke as compared to sham controls that persisted for up to 10 days after stroke (Fig. 2F; day
 470 10: $-15.4 \pm 6.4\%$; $F(2, 70) = 13.82$, $p < 0.0001$; two-way ANOVA, followed by Bonferroni
 471 post-hoc test). These findings are consistent with hemispheric stroke in rodents and human
 472 subjects (Ahmed et al., 2011; Poryazova et al., 2015). Moreover, the SW positive slope was
 473 reduced within the ipsilateral area of Stroke animals (Fig. 2G; $F(2, 76) = 13.02$, $p < 0.0001$),

474 whereas the negative slope increased (Fig. 2H; $F(2, 76) = 15.89$, $p < 0.0001$). No significant
 475 changes were found in the number of detected SW (Fig. 2I; $F(2, 87) = 0.693$, $p = 0.503$) or
 476 their duration (Fig. 2J; $F(82, 83) = 0.744$, $p = 0.478$; two-way ANOVA, followed by Tukey
 477 post-hoc test). When exploring for a homeostatic effect, we did not find differences in
 478 amplitude between Stroke and Sham for ipsi- and contralateral EEG traces ($LR(2) = 0.940$, p
 479 $= 0.625$) nor for *time of night* ($LR(2) = 3.791$, $p = 0.150$).

480 **SW^{opto} revealed a critical window of intervention after stroke**

481 Here, we aimed at identifying the effect of optogenetically-induced SW (SW^{opto}) on the
 482 recovery of motor function following MCAo stroke in mice. Thus, we genetically targeted
 483 the expression of opsins to pyramidal neurons in layer V of the neocortex, given their
 484 implication in the generation of slow oscillations (McCormick et al., 2015; Beltramo et al.,
 485 2013). To achieve this, we stereotactically infused AAV2 viruses carrying ChR2, ArchT or
 486 mCherry gene cassettes under CaMKII promoter in iS1FL (Fig. 3A, B) before animals were
 487 chronically implanted with EEG/EMG electrodes, tetrodes in cS1FL, iM1 and cM1 cortices
 488 (layer V) and a single optrode in iS1FL (see above and Methods, Fig. 3A). We first optimized
 489 the frequency and duration of optogenetic stimulations to mimic NREM sleep SW in both
 490 wild type and VGAT-Cre transgenic mice to modulate excitatory or inhibitory neurons in
 491 iS1FL with 5 Hz, 1 ms light pulses (activation protocol) or 100, 200, 500 ms single pulses
 492 (silencing protocol) (Fig. 4). We found that 5 ms optogenetic activation of iS1FL ChR2-
 493 expressing pyramidal neurons induced a short UP-like state followed by a DOWN-like state,
 494 indistinguishable from spontaneous NREM sleep SW (Fig. 3C-E). Similar SW^{opto} waveform
 495 profiles were obtained upon 200 ms optogenetic silencing of iS1FL ArchT-expressing
 496 pyramidal neurons (Fig. 3F, I). In the latter condition, the duration of the optogenetic
 497 silencing of iS1FL ArchT-expressing pyramidal neurons corresponded to the average

499 duration of spontaneous NREM sleep DOWN states (Fig. 2C; duration: 205.2 ± 4.4 ms; Fig.
 500 3H). Off-line analysis confirmed that SW^{opto} duration, negative amplitude and slope were
 501 indistinguishable from naturally occurring NREM sleep SW from the same animal (Fig. 3E,
 502 I). SW^{opto} propagated to contralateral recording sites, where SW^{opto} of variable amplitudes
 503 were recorded in EEG, LFP and single activity traces (Fig. 3D, H and Fig. 5). No changes in
 504 EEG features were observed in control conditions (Fig. 3J-L).

505
 506 To determine the optimal window for optogenetic intervention after MCAo, we evaluated the
 507 effect of this stimulation parameters on the survival rates of stroke animals. Strikingly, we
 508 observed that $ChR2^{stroke}$ animals had lower survival rate than $ArchT^{stroke}$ and $mCherry^{stroke}$
 509 mice when the optogenetic manipulation started on post-stroke day 1 (single 5 or 200 ms
 510 light pulses, at 473 nm or 532 nm, respectively, randomly distributed over 2 h, daily; Fig. 6A;
 511 Chi square(2) = 7.941, $p = 0.018$; $ChR2^{stroke}$: 30% survival; $ArchT^{stroke}$: 75% survival;
 512 $mCherry^{stroke}$: 77.7% survival; Log-rank Mantel-Cox test), as compared to day 5 (Fig. 6B;
 513 Chi square(4) = 6.383, $P = 0.172$; $ChR2^{stroke}$: 60% survival; $ArchT^{stroke}$: 70% survival;
 514 $mCherry^{stroke}$: 70% survival; $mCherry^{sham}$: 100 % survival; Naive: 100 % survival; Long-rank
 515 Mantel-Cox test). These findings are consistent with an increased excitotoxicity after stroke
 516 (Nudo, 2006; Allman et al., 2016), hence, all our optogenetic experiments started on day 5.

517 **SW^{opto} during sleep improves functional recovery**

518
 519 We next tested whether sleep-specific SW^{opto} improves functional recovery after MCAo in
 520 mice. The expression of $ChR2$, $ArchT$ and $mCherry$ was genetically targeted to iS1FL
 521 pyramidal neurons as described above (Fig. 3A) before animals were chronically implanted
 522 with a unilateral optic fiber on iS1FL and EEG/EMG electrodes for simultaneous optogenetic
 523 control and polysomnographic recordings in freely moving mice (Fig. 7A; see Methods).

Sparse SW^{opto} were randomly distributed during sleep starting 5 days after stroke until day 15
 (single 5 or 200 ms light pulses, at 473 nm or 532 nm, respectively, randomly distributed
 over 2 h, daily; $n \sim 300$ optical stimuli; Fig. 7B, C).

Evaluation of the animals' fine motor movements, coordination, strength and asymmetry at
 post-stroke day 4 (Fig. 7B) showed severe behavioural deficits in all animals subjected to
 MCAo. Indeed, on post-stroke day 4 stroke-induced animals were no longer able to finely
 coordinate their grasping movements (Fig. 7D; $LR(1) = 27.498$, $p < 0.0001$; Fig. 7F; $LR(1) =$
 32.205 , $p < 0.0001$). As expected, no behavioural impairments were found in mCherry^{sham}
 and Naive animals (Fig. 7D; F, respectively, $p > 0.05$).

In the ladder walking rig test (Fig. 7D), a significant interaction between the *stimulation*
group and *days* was found ($LR(5) = 11.976$, $p = 0.035$). Post-hoc analysis revealed that the
 ArchT^{stroke} group recovered at a faster pace than ChR2^{stroke_wake} ($t(101) = 2.842$, $p = 0.005$).
 Generally all mice improved across days ($LR(6) = 28.235$, $p < 0.001$). Main effects of
 stimulation group were also found ($LR(10) = 42.949$, $p < 0.001$). ChR2^{stroke}, ChR2^{stroke_wake}
 were significantly different from mCherry^{stroke} ($t(101) = -2.430$, $p = 0.017$; $t(101) = -3.137$, p
 $= 0.002$). For the beam balance (Fig. 7F) we found a significant interaction effect of
stimulation group and *day* ($LR(5) = 14.171$, $p = 0.015$). mCherry^{stroke} did not show a
 significant improvement across days ($t(152) = -1.671$, $p = 0.097$). However, compared to
 mCherry^{stroke}, ArchT^{stroke} mice showed significantly more improvement over the course of
 days ($t(110) = -2.866$, $p = 0.005$). ChR2^{stroke} mice also significantly improved across days
 after stroke ($t(152) = -4.168$, $p < 0.001$), but this improvement was less than the ArchT^{stroke}
 group ($t(110) = -2.285$, $p = 0.024$) and on par with the mCherry^{stroke} group ($t(110) = 0.580$, p
 $= 0.563$). Comparisons of animal improvement between post-stroke day 4 and 15 confirmed
 the functional recovery of ChR2^{stroke} (Fig. 7E; $t(14) = 3.46$, $p = 0.007$; Fig. 7G; $t(18) = 2.372$,

549 $p = 0.029$) and ArchT^{stroke} (Fig. 7E; $t(14) = 3.083$, $p = 0.008$; Fig. 7G; $t(18) = 3.895$ $p =$
 550 0.002 ; one-way ANOVA), in comparison to mCherry^{stroke} control. In contrast, optogenetic
 551 intervention after stroke did not lead to any improvement of motor endurance, strength (Fig.
 552 7H) or asymmetry (Fig. 7I).

554 **SW^{opto} increases axonal sprouting**

555 Stroke triggers a cascade of molecular and cellular changes including synaptogenesis,
 556 neurogenesis and axonal sprouting in peri-infarct zone and remote connected circuits (Nudo,
 557 1997; Carmichael et al., 2017).

558 To quantify the anatomical changes induced by chronic SW^{opto}, we quantified the expression
 559 of pre-synaptic Vglut1 and post-synaptic PSD-95 proteins as a direct measurement of axonal
 560 sprouting in cortical layers V (Liu et al., 2007; Sun et al., 2017) and connected circuits in
 561 layers II (Binzegger et al., 2004; Adesnik and Naka, 2018) (Fig. 8A). Puncta density
 562 quantification in both iS1FL and cS1FL cortices revealed a significantly higher Vglut1
 563 protein levels in ipsilateral layer II (Fig. 8B; $F(3, 19) = 10.49$, $p = 0.0003$), and layer V (Fig.
 564 8C; $F(3, 18) = 16.02$, $p > 0.0001$; one-way ANOVA) from ChR2^{stroke} and ArchT^{stroke} animals,
 565 as compared to mCherry controls. Consistently, analysis of Vglut1 positive puncta volume
 566 distribution revealed a significant increase of smaller, newly-formed puncta within ipsilateral
 567 layer V of both ArchT^{stroke} and ChR2^{stroke} as compared to mCherry^{stroke} animals (Fig. 8E; $F(2,$
 568 $2111) = 75.13$, $p < 0.0001$). This was also true for *ex novo* Vglut1 puncta in post-synaptic
 569 sites of layer II from ChR2^{stroke} animals (Fig. 8D; mCherry^{stroke} vs. ChR2^{stroke} $t(2070) = 4.181$,
 570 $p < 0.0001$), but not ArchT^{stroke} animals (mCherry^{stroke} vs. ArchT^{stroke} $t(2070) = 3.015$, $p =$
 571 0.0078 , ChR2^{stroke} vs. ArchT^{stroke} $t(2070) = 0.903$, $p > 0.999$; one-way ANOVA, followed by
 572 Bonferroni correction).

573 These pre-synaptic changes were concomitant to a significant decrease of post-synaptic PSD-
 574 95 protein expression in iS1FL layer II of both ChR2 and ArchT expressing animals when
 575 compared to control group (Fig. 8F; $F(3, 23) = 8.609$, $p = 0.0005$; one-way ANOVA), with
 576 no differences in layer V (Fig. 8G; $F(3, 24) = 1.095$, $p = 0.370$; one-way ANOVA). PSD-95
 577 positive puncta volume were significantly larger iS1FL layer II (Fig. 8H; $F(2, 625) = 85$, $p <$
 578 0.0001) and layer V from ChR2^{stroke} animal as compared to mCherry^{stroke} or ArchT^{stroke} (Fig.
 579 8I; $F(2, 2111) = 75.13$, $p < 0.0001$; one-way ANOVA).

580

581

582 **DISCUSSION**

583 Stroke is a debilitating neurological disorder and one of the worldwide leading causes of
 584 adult disability and death in aging population. A better understanding of the complex
 585 pathophysiological mechanisms underlying the stroke event and the following brain plasticity
 586 warrants the improvement of existing strategies and the development of alternative therapies
 587 for stroke recovery (Feigin et al., 2017).

588 Here, we showed that MCAo induced an ipsilateral reduction of spontaneous SW amplitude,
 589 associated with sleep fragmentation and increased NREM sleep after stroke onset (Giubilei et
 590 al., 1992; Vock et al., 2002; Baumann et al., 2006; Hermann et al., 2008). Our results further
 591 indicate that sleep-specific optogenetic neuromodulation of brain activity after stroke had no
 592 effects on the sleep-wake cycle architecture, but it improved fine skilled motor movements in
 593 comparison to wakefulness interventions. These manipulations were accompanied by axonal
 594 sprouting of local and connected circuits, suggesting a direct role for SW in promoting
 595 anatomical and functional plasticity of neural circuit during sleep (Carmichael and Chesselet,
 596 2002; Aeschbach et al., 2008; Tononi and Cirelli, 2014). Collectively, these findings
 597 emphasize a role for NREM sleep SW as a window of intervention during stroke recovery

598 and a possible mechanism underlying the improvement of rehabilitative strategies using
 599 repetitive transcranial magnetic stimulation (rTMS) (Kim et al., 2006; Brodie et al., 2014)
 600 and transcranial direct current stimulation (tDCS) (Boggio et al., 2006; Lindenberg et al.,
 601 2010).

602

603 Spontaneous sleep SW are associated with neuroplastic changes (Tononi and Cirelli, 2006;
 604 Puentes-Mestril and Aton, 2017), inflammatory and immunological adaptative response
 605 (Irwin and Cole, 2011), protective functions during infection (Irwin, 2019), metabolic
 606 clearance (Xie et al., 2013). Clinical studies reported significant improvement in stroke
 607 rehabilitation upon non-invasive brain stimulation during sleep (Niimi et al., 2018) and SW
 608 enhancement (Ebajemito et al., 2016). We used physiologically-relevant stimulation
 609 protocols to avoid neuronal hypersynchrony, un-natural firing activities and circuit adaptation
 610 by using single optogenetic stimuli randomly distributed across sleep in freely-moving
 611 animals. These sparse optogenetics interventions induced SW^{opto} without perturbing sleep-
 612 wake cycle architecture. Our strategy contrasts from other studies that use long-lasting
 613 hypersynchronous optogenetic activation independently of the animal behaviour, sleep-wake
 614 states, or delivered during anaesthesia (Cheng et al., 2014; Shah et al., 2017; Tennant et al.,
 615 2017; Lu et al., 2017). Our findings show that sparse SW^{opto} delivered during sleep improved
 616 behavioural outcomes whereas SW^{opto} during wakefulness did not. An explanation for this
 617 striking difference is that low frequency, high amplitude waves during wakefulness represent
 618 dysfunctional waves, typical of pathological conditions that are often associated with
 619 functional abnormalities, including deafferented or lesioned thalamo-cortical circuits
 620 (Steriade et al., 1993; Butz et al., 2004). These results further emphasize the importance of
 621 sleep as a window for optimal modulation of brain activity that potentiates the effect of
 622 SW^{opto} on brain plasticity and behavioural outcomes (see below).

623

624 *Alteration of sleep-wake cycle and slow wave*

625 Our findings showed that stroke injury induces a dramatic increase in NREM sleep on the
 626 day following stroke. This effect is accompanied by transient perturbation of the circadian
 627 sleep distribution across the light/ dark cycle. Although the causes of these transient changes
 628 remain unclear, they may result from a functional adaptation to the strong fragmentation of
 629 both NREM sleep and wakefulness.

630 Our experimental results are consistent with the sleep fragmentation, the increase in NREM
 631 sleep stages 1-2 and the decreased REM sleep observed during the first days following stroke
 632 in human (Giubilei et al., 1992; Vock et al., 2002). Sleep fragmentation may result from a
 633 lack of consolidated synchrony of neuronal activity amongst thalamo-cortical circuitries, as
 634 suggested by the decreased amplitude and positive slope of spontaneous SW after stroke
 635 observed in our study. These SW profiles are indicative of low spiking synchrony of thalamic
 636 and cortical neurons (Huber et al., 2004; Vyazovskiy et al., 2009), which may facilitate
 637 arousal upon wake-promoting inputs of sub-cortical origins (Adamantidis et al., 2007; Carter
 638 et al., 2010; Herrera et al., 2016; Gent et al., 2018). Whether the SW remaining after stroke
 639 are generated by a similar mechanism and support similar cortical functions, as the
 640 naturalistic SW recorded from an intact brain remains to be examined in light of the different
 641 cells types potentially implicated in SW generation (Gerashchenko et al., 2008; Cardin et al.,
 642 2009; Stroh et al., 2013; Jackson et al., 2016; Niethard et al., 2016). An important
 643 characteristic of spontaneous sleep SW is their propagation pattern across the brain cortex,
 644 originating at anterior regions and travelling to posterior directions (Massimini et al., 2004,
 645 Gent et al., 2018). Investigating SW's traveling changes across the ipsi-lateral hemisphere
 646 and the peri-infarct zone specifically represents an interesting additional aspect to explore in

647 future work. The experimental preparation of the present study (single EEG trace per
648 hemisphere) limited further SW analysis in this direction.

649

650 *SW^{opto} promotes behavioural recovery after stroke*

651 Chronic SW^{opto} over 11 days after stroke facilitated spontaneous functional recovery, while
652 earlier interventions exacerbated brain injury and decreased the survival rate of the animals,
653 possibly due to excessive glutamate release (Lai et al., 2014) leading to increased
654 excitotoxicity (Nudo, 2006; Allman et al., 2016). This window of spontaneous recovery is
655 limited to a month in rodents, and three months in humans, during which molecular and
656 structural changes potentiate the responsiveness to rehabilitative treatments (Murphy and
657 Corbett, 2009; Ng et al., 2015) and emphasize a crucial intervention timeframe (Dromerick et
658 al., 2009). Although post-stroke excitotoxicity might be an accurate explanation for the
659 detrimental effect observed in animals' survival, additional studies are required to further
660 scrutinize markers of excitotoxicity (e.g. levels of glutamate, NMDA receptors, AMPA
661 receptors and their activation, caspases, reactive oxygen species) in combination with
662 optogenetic intervention at several time points following stroke.

663

664 An interesting finding in our study is that SW^{opto} had no direct effects on sleep architecture
665 but induced a delayed increase of sleep duration. This result is in agreement with studies
666 showing prolonged NREM sleep upon activation of somatostatin interneurons (Funk et al.,
667 2017), and to a lesser extent pyramidal neurons (Rodriguez et al., 2016) in the neocortex.
668 Noteworthy, increased NREM sleep following SW^{opto} intervention was present only within
669 the first two days of stimulation (not shown), presumably due to the brain recovery processes
670 or the adaptation of the sleep-promoting circuits to the SW^{opto}, or both. Although we cannot
671 rule out a possible role of this transient NREM sleep increase on the sensorimotor

improvement of the animals, it is unlikely that these early and transient changes are responsible for the motor improvements observed at the end of the experiment.

Slow wave, plasticity and axonal sprouting

In our experiments, sensorimotor improvement after stroke was achieved by either chronic optogenetic activation, or silencing, of iS1FL pyramidal neurons in freely-moving mice, supporting an essential role for UP-DOWN states, rather than neuronal activation or silencing alone, in brain plasticity (Puentes-Mestril and Aton, 2017). These bistable states during NREM sleep (here, mainly SW^{opto}) are associated with synaptic plasticity in local circuits and their postsynaptic targets, as observed for the beneficial effect of sleep low frequency stimulation of motor or somatosensory cortical circuits on perceptual learning (Miyamoto et al., 2016) or the formation of new dendritic spines in motor cortex (layer V) pyramidal neurons in mice (Yang et al., 2014). Furthermore, our results are in agreement with the finding that experimental disruption of cortical SW following learning impairs consolidation of visuomotor learning in human (Landsness et al., 2009).

The early stages of stroke recovery are classically attributed to brain oedema resorption and penumbra reperfusion, while later stages are associated with structural reorganization through axonal sprouting, synaptogenesis and neurogenesis (Nudo, 2006). Here, both ChR2-, and to a lesser extent ArchT-induced SW^{opto} promoted an increase of pre- and post-synaptic markers in S1FL layers V and II respectively. Decreased PSD-95 density after SW^{opto} is consistent with similar findings upon rTMS stimulation in rodents (Etiévant et al., 2015) that correlate with improved functional outcomes in non-human primates treated with PSD-95 inhibitors (Cook et al., 2012). Larger PSD-95 puncta were found within both layers II and V of ChR2^{stroke} animals, suggestive of a stabilization of the functional synapse (Cane et al., 2014).

697 Thus, SW^{opto} enhance UP/ DOWN state network synchronization (Gent et al., 2018) and
698 facilitate the formation of new synapses which are not restricted to targeted cortical circuits
699 (i.e. pyramidal neurons in the peri-infarct zone) but also anatomically connected circuits
700 located in ipsi- and contra-lateral hemispheres (Liu et al., 2009; Cui et al., 2013).
701 Noteworthy, brain activity in other cortical and sub-cortical networks and other sleep
702 oscillations including spindles participate to synaptic plasticity during NREM sleep
703 (Rosanova and Ulrich, 2005; Chauvette et al., 2012) and may contribute to the behavioral
704 outcome reported here.

705

706 Collectively, our findings support a role for NREM sleep SW in neuronal circuit plasticity
707 and provide a clinically-relevant framework for developing sparse, non-invasive
708 neuromodulation, including acoustic brain stimulations (Ngo et al., 2013), TMS or tDCS
709 (Ebajemito et al., 2016; Niimi et al., 2018) for optimal recovery after brain injury.

710

711 **REFERENCES**

- 712 Adamantidis AR, Zhang F, Aravanis AM, Deisseroth K, de Lecea L (2007) Neural substrates
713 of awakening probed with optogenetic control of hypocretin neurons. *Nature* 450:420–
714 424.
- 715 Adesnik H, Naka A (2018) Cracking the Function of Layers in the Sensory Cortex. *Neuron*
716 100:1028–1043.
- 717 Aeschbach D, Cutler AJ, Ronda JM (2008) A Role for Non-Rapid-Eye-Movement Sleep
718 Homeostasis in Perceptual Learning. *J Neurosci* 28:2766–2772.
- 719 Ahmed S, Meng H, Liu T, Sutton BC, Opp MR, Borjigin J, Wang MM (2011) Ischemic
720 stroke selectively inhibits REM sleep in rats. *Exp Neurol* 232:168–75.
- 721 Allman C, Amadi U, Winkler AM, Wilkins L, Filippini N, Kischka U, Stagg CJ, Johansen-
722 Berg H (2016) Ipsilesional anodal tDCS enhances the functional benefits of
723 rehabilitation in patients after stroke. *Sci Transl Med* 8:1–21.
- 724 Ameli M, Grefkes C, Kemper F, Riegg FP, Rehme AK, Karbe H, Fink GR, Nowak DA
725 (2009) Differential effects of high-frequency repetitive transcranial magnetic stimulation
726 over ipsilesional primary motor cortex in cortical and subcortical middle cerebral artery
727 stroke. *Ann Neurol* 66:298–309.
- 728 Asanuma H, Arissian K (1984) Experiments on functional role of peripheral input to motor
729 cortex during voluntary movements in the monkey. *J Neurophysiol* 52:212–227.
- 730 Baglioni C, Nissen C, Schweinich A, Riemann D, Spiegelhalder K, Berger M, Weiller C,
731 Sterr A (2016) Polysomnographic characteristics of sleep in stroke: A Systematic review
732 and meta- analysis. *PLoS One* 11:1–23.
- 733 Balkaya M, Kröber JM, Rex A, Endres M (2013) Assessing post-stroke behavior in mouse
734 models of focal ischemia. *J Cereb Blood Flow Metab* 33:330–338.
- 735 Baumann CR, Kilic E, Petit B, Werth E, Hermann DM, Tafti M, Bassetti CL (2006) Sleep

- 736 EEG changes after middle cerebral artery infarcts in mice: Different effects of striatal
737 and cortical lesions. *Sleep* 29:1339–1344.
- 738 Beltramo R, D’Urso G, Dal Maschio M, Farisello P, Bovetti S, Clovis Y, Lassi G, Tucci V,
739 De Pietri Tonelli D, Fellin T (2013) Layer-specific excitatory circuits differentially
740 control recurrent network dynamics in the neocortex. *Nat Neurosci* 16:227–234.
- 741 Binzegger T, Douglas RJ, Martin KAC (2004) A Quantitative Map of the Circuit of Cat
742 Primary Visual Cortex. *J Neurosci* 24:8441–8453.
- 743 Boggio PS, Nunes A, Rigonatti SP, Nitsche MA, Pascual-Leone A, Fregni F (2006) Repeated
744 sessions of noninvasive brain DC stimulation is associated with motor function
745 improvement in stroke patients. *Restor Neurol Neurosci* 25:123–139.
- 746 Brochier T, Boudreau MJ, Paré M, Smith AM (1999) The effects of muscimol inactivation of
747 small regions of motor and somatosensory cortex on independent finger movements and
748 force control in the precision grip. *Exp Brain Res* 128:31–40.
- 749 Brodie SM, Meehan S, Borich MR, Boyd LA (2014) 5 Hz repetitive transcranial magnetic
750 stimulation over the ipsilesional sensory cortex enhances motor learning after stroke.
751 *Front Hum Neurosci* 8:1–10.
- 752 Brooks SP, Dunnett SB (2009) Tests to assess motor phenotype in mice: A user’s guide. *Nat*
753 *Rev Neurosci* 10:519–529.
- 754 Butz M, Gross J, Timmermann L, Moll M, Freund HJ, Witte OW, Schnitzler A (2004)
755 Perilesional pathological oscillatory activity in the magnetoencephalogram of patients
756 with cortical brain lesions. *Neurosci Lett* 355:93–96.
- 757 Cane M, Maco B, Knott G, Holtmaat A (2014) The Relationship between PSD-95 Clustering
758 and Spine Stability In Vivo. *J Neurosci* 34:2075–2086.
- 759 Cardin JA, Carlén M, Meletis K, Knoblich U, Zhang F, Deisseroth K, Tsai LH, Moore CI
760 (2009) Driving fast-spiking cells induces gamma rhythm and controls sensory responses.

- 761 Nature 459:663–667.
- 762 Carmichael ST (2012) Brain excitability in stroke: The yin and yang of stroke progression.
- 763 Arch Neurol 69:161–167.
- 764 Carmichael ST, Chesselet M-F (2002) Synchronous neuronal activity is a signal for axonal
- 765 sprouting after cortical lesions in the adult. J Neurosci 22:6062–6070.
- 766 Carmichael ST, Kathirvelu B, Schweppe CA, Nie EH (2017) Molecular, cellular and
- 767 functional events in axonal sprouting after stroke. Exp Neurol 287:384–394.
- 768 Carter ME, Yizhar O, Chikahisa S, Nguyen H, Adamantidis A, Nishino S, Deisseroth K, De
- 769 Lecea L (2010) Tuning arousal with optogenetic modulation of locus coeruleus neurons.
- 770 Nat Neurosci 13:1526–1535.
- 771 Chauvette S, Seigneur J, Timofeev I (2012) Sleep Oscillations in the Thalamocortical System
- 772 Induce Long-Term Neuronal Plasticity. Neuron 75:1105–1113.
- 773 Cheng MY, Wang EH, Woodson WJ, Wang S, Sun G, Lee AG, Arac A, Fenno LE,
- 774 Deisseroth K, Steinberg GK (2014) Optogenetic neuronal stimulation promotes
- 775 functional recovery after stroke. Proc Natl Acad Sci 111:12913–12918.
- 776 Cook DJ, Teves L, Tymianski M (2012) Treatment of stroke with a PSD-95 inhibitor in the
- 777 gyrencephalic primate brain. Nature 483:213–217.
- 778 Csercsa R et al. (2010) Laminar analysis of slow wave activity in humans. Brain 133:2814–
- 779 2829.
- 780 Cui L, Murikinati SR, Wang D, Zhang X, Duan WM, Zhao LR (2013) Reestablishing
- 781 Neuronal Networks in the Aged Brain by Stem Cell Factor and Granulocyte-Colony
- 782 Stimulating Factor in a Mouse Model of Chronic Stroke. PLoS One 8:2–12.
- 783 Cummings BJ, Engesser-Cesar C, Cadena G, Anderson AJ (2007) Adaptation of a ladder
- 784 beam walking task to assess locomotor recovery in mice following spinal cord injury.
- 785 Behav Brain Res 177:232–241.

- 786 Doeppner TR, El Aanbouri M, Dietz GPH, Weise J, Schwarting S, Bähr M (2010)
 787 Transplantation of TAT-Bcl-xL-transduced neural precursor cells: Long-term
 788 neuroprotection after stroke. *Neurobiol Dis* 40:265–276.
- 789 Doyon J (2008) Motor sequence learning and movement disorders. *Curr Opin Neurol*
 790 21:478–483.
- 791 Dromerick AW, Birkenmeier RL, Miller JP, Videen TO, Power WJ, Wolf SL, Edwards DF
 792 (2009) Very Early Constraint-Induced Movement during Stroke Rehabilitation (
 793 VECTORS). *Neurology* 73:195–201.
- 794 Duss SB, Seiler A, Schmidt MH, Pace M, Adamantidis A, Müri RM, Bassetti CL (2017) The
 795 role of sleep in recovery following ischemic stroke: A review of human and animal data.
 796 *Neurobiol Sleep Circadian Rhythm* 2:94–105.
- 797 Ebajemito JK, Furlan L, Nissen C, Sterr A (2016) Application of transcranial direct current
 798 stimulation in neurorehabilitation: The modulatory effect of sleep. *Front Neurol* 7:54.
- 799 Etiévant A, Manta S, Latapy C, Magno LA V., Fecteau S, Beaulieu JM (2015) Repetitive
 800 transcranial magnetic stimulation induces long-lasting changes in protein expression and
 801 histone acetylation. *Sci Rep* 5:1–9.
- 802 Feigin VL, Norrving B, Mensah GA (2017) Global Burden of Stroke. *Circ Res* 120:439–448.
- 803 Fernández-Bouzas a, Harmony T, Fernández T, Aubert E, Ricardo-Garcell J, Valdés P, Bosch
 804 J, Casián G, Sánchez-Conde R (2002) Sources of Abnorma EEG Activityin Spontaneous
 805 Intracerebral Hemorrhage. *Clin EEG Neurosci* 33:70-76.
- 806 Funk CM, Peelman K, Bellesi M, Marshall W, Cirelli C, Tononi G (2017) Role of
 807 Somatostatin-Positive Cortical Interneurons in the Generation of Sleep Slow Waves. *J*
 808 *Neurosci* 37:9132–9148.
- 809 Gao B, Kilic E, Baumann CR, Hermann DM, Bassetti CL (2008) Gamma-hydroxybutyrate
 810 accelerates functional recovery after focal cerebral ischemia. *Cerebrovasc Dis* 26:413–

- 811 419.
- 812 Gent TC, Bandarabadi M, Herrera CG, Adamantidis AR (2018) Thalamic dual control of
- 813 sleep and wakefulness. *Nat Neurosci* 21:1–11.
- 814 Gerashchenko D, Wisor JP, Burns D, Reh RK, Shiromani PJ, Sakurai T, de la Iglesia HO,
- 815 Kilduff TS (2008) Identification of a population of sleep-active cerebral cortex neurons.
- 816 *Proc Natl Acad Sci* 105:10227–10232.
- 817 Giubilei F, Iannilli M, Vitale A, Pierallini A, Sacchetti ML, Antonini G, Fieschi C (1992)
- 818 Sleep patterns in acute ischemic stroke. *Acta Neurol Scand* 86:567–571.
- 819 Grefkes C, Fink GR (2014) Connectivity-based approaches in stroke and recovery of
- 820 function. *Lancet Neurol* 13:206–216.
- 821 Hermann DM, Siccoli M, Brugger P, Wachter K, Mathis J, Achermann P, Bassetti CL (2008)
- 822 Evolution of Neurological, Neuropsychological and Sleep-Wake Disturbances After
- 823 Paramedian Thalamic Stroke. *Stroke* 39:62–68.
- 824 Herrera CG, Cadavieco MC, Jegu S, Ponomarenko A, Korotkova T, Adamantidis A (2016)
- 825 Hypothalamic feedforward inhibition of thalamocortical network controls arousal and
- 826 consciousness. *Nat Neurosci* 19:290–298.
- 827 Hodor A, Palchykova S, Baracchi F, Noain D, Bassetti CL (2014) Baclofen facilitates sleep,
- 828 neuroplasticity, and recovery after stroke in rats. *Ann Clin Transl Neurol* 1:765–777.
- 829 Huang J, Upadhyay UM, Tamargo RJ (2006) Inflammation in stroke and focal cerebral
- 830 ischemia. *Surg Neurol* 66:232–245.
- 831 Huber R, Ghilardi MF, Massimini M, Tononi G (2004) Local sleep and learning. *Nature*
- 832 430:78–81.
- 833 Irwin MR (2019) Sleep and inflammation: partners in sickness and in health. *Nat Rev*
- 834 *Immunol* 19:702–715.
- 835 Irwin MR, Cole SW (2011) Reciprocal regulation of the neural and innate immune systems.

- 836 Nat Rev Immunol 11:625–632.
- 837 Jackson J, Ayzenshtat I, Karnani MM, Yuste R (2016) VIP+ interneurons control neocortical
838 activity across brain states. J Neurophysiol 115:3008–3017.
- 839 Jegu S, Glasgow SD, Herrera CG, Ekstrand M, Reed SJ, Boyce R, Friedman J, Burdakov D,
840 Adamantidis AR (2013) Optogenetic identification of a rapid eye movement sleep
841 modulatory circuit in the hypothalamus. Nat Neurosci 16:1637–1643.
- 842 Kaneko Y, Floras JS, Usui K, Plante J, Tkacova R, Kubo T, Ando S, Bradley TD (2003)
843 Cardiovascular Effects of Continuous Positive Airway Pressure in Patients with Heart
844 Failure and Obstructive Sleep Apnea. N Engl J Med 348:1233–1241.
- 845 Khedr EM, Ahmed MA, Fathy N, Rothwell JC (2005) Therapeutic trial of repetitive
846 transcranial magnetic stimulation after acute ischemic stroke. Neurology 65:466–468.
- 847 Kielar A, Deschamps T, Chu RKO, Jokel R, Khatamian YB, Chen JJ, Meltzer JA (2016)
848 Identifying dysfunctional cortex: Dissociable effects of stroke and aging on resting state
849 dynamics in MEG and fmri. Front Aging Neurosci 8:40.
- 850 Kim YH, You SH, Ko MH, Park JW, Lee KH, Jang SH, Yoo WK, Hallett M (2006)
851 Repetitive transcranial magnetic stimulation-induced corticomotor excitability and
852 associated motor skill acquisition in chronic stroke. Stroke 37:1471–1476.
- 853 Lai TW, Zhang S, Wang YT (2014) Excitotoxicity and stroke: Identifying novel targets for
854 neuroprotection. Prog Neurobiol:157–188.
- 855 Landsness EC, Crupi D, Hulse BK, Peterson MJ, Huber R, Ansari H (2009) Sleep-Dependent
856 Improvement in Visuomotor Learning: A Causal Role for Slow Waves. Sleep 32:123–
857 184.
- 858 Liew S-L, Santarnecchi E, Buch ER, Cohen LG (2014) Non-invasive brain stimulation in
859 neurorehabilitation: local and distant effects for motor recovery. Front Hum Neurosci
860 8:378.

- 861 Lin TN, He YY, Wu G, Khan M, Hsu CY (1993) Effect of brain edema on infarct volume in
862 a focal cerebral ischemia model in rats. *Stroke* 24:117–121.
- 863 Lindenberg R, Renga V, Zhu LL, Nair D, Schlaug G (2010) Bihemispheric brain stimulation
864 facilitates motor recovery in chronic stroke patients. *Neurology* 75:2176–2184.
- 865 Liu Z, Li Y, Qu R, Shen L, Gao Q, Zhang X, Lu M, Savant-Bhonsale S, Borneman J, Chopp
866 M (2007) Axonal sprouting into the denervated spinal cord and synaptic and
867 postsynaptic protein expression in the spinal cord after transplantation of bone marrow
868 stromal cell in stroke rats. *Brain Res* 1149:172–180.
- 869 Liu Z, Zhang RL, Li Y, Cui Y, Chopp M (2009) Remodeling of the corticospinal innervation
870 and spontaneous behavioral recovery after ischemic stroke in adult mice. *Stroke*
871 40:2546–2551.
- 872 Lu Y, Jiang L, Qu M, Song Y, He X, Zhang Z, Yang G-Y, Wang Y (2017) Optogenetic
873 inhibition of striatal neurons improves the survival of implanted neural stem cell and
874 neurological outcomes after ischemic stroke in mice. *Stem Cells Int* 2017:11.
- 875 Massimini M, Huber R, Ferrarelli F, Hill S, Tononi G (2004) The Sleep Slow Oscillation as a
876 Traveling Wave. *J Neurosci Res* 24:6862–6870.
- 877 McCormick DA, McGinley MJ, Salkoff DB (2015) Brain state dependent activity in the
878 cortex and thalamus. *Curr Opin Neurobiol* 31:133–140.
- 879 Mensen A, Riedner B, Tononi G (2016) Optimizing detection and analysis of slow waves in
880 sleep EEG. *J Neurosci Methods* 274:1–12.
- 881 Miyamoto D, Jirai D, Fung CCA, Inutsuka A, Odagawa M, Suzuki T, Boehringer R,
882 Adaikkan C, Matsubara C, Matsuki N, Fukai T, McHugh TJ, Yamanaka A, Murayama
883 (2016) Top-down cortical input during NREM sleep consolidates perceptual memory.
884 *Science* 352:1315–1318.
- 885 Murphy TH, Corbett D (2009) Plasticity during stroke recovery: from synapse to behaviour.

- 886 Nat Rev Neurosci 10:861–872.
- 887 Murri L, Gori S, Massetani R, Bonanni E, Marcella F, Milani S (1998) Evaluation of acute
888 ischemic stroke using quantitative EEG: A comparison with conventional EEG and CT
889 scan. *Neurophysiol Clin* 28:249-257.
- 890 Ng K, Gibson EM, Hubbard R, Yang J, Caffo B, O'Brien R, Krakauer JW, Zeiler SR (2015)
891 Fluoxetine maintains a state of heightened responsiveness to motor training early after
892 stroke in a mouse model Kwan. *Stroke* 46:2951–2960.
- 893 Ngo HV V., Claussen JC, Born J, Mölle M (2013) Induction of slow oscillations by rhythmic
894 acoustic stimulation. *J Sleep Res* 22:22–31.
- 895 Niethard N, Hasegawa M, Itokazu T, Oyanedel CN, Born J, Sato TR (2016) Sleep-Stage-
896 Specific Regulation of Cortical Excitation and Inhibition. *Curr Biol* 26:2739–2749.
- 897 Niimi M, Sasaki N, Kimura C, Hara T, Yamada N, Abo M (2018) Sleep during low-
898 frequency repetitive transcranial magnetic stimulation is associated with functional
899 improvement in upper limb hemiparesis after stroke. *Acta Neurol Belg* 119:1–6.
- 900 Nudo RJ (1997) Remodeling of cortical motor representations after stroke: implications for
901 recovery from brain damage. *Mol Psychiatry* 2:188–191.
- 902 Nudo RJ (2006) Mechanisms for recovery of motor function following cortical damage. *Curr*
903 *Opin Neurobiol* 16:638–644.
- 904 Panagiotou M, Vyazovskiy V V., Meijer JH, Deboer T, Czeisler CA (2017) Differences in
905 electroencephalographic non-rapid-eye movement sleep slow-wave characteristics
906 between young and old mice. *Sci Rep* 7:43656.
- 907 Park SY, Marasini S, Kim GH, Ku T, Choi C, Park MY, Kim EH, Lee YD, Suh-kim H, Kim
908 SS (2014) A method for generate a mouse model of stroke: evaluation of parameters for
909 blood flow, behavior, and survival. *Exp Neurobiol* 23:104–114.
- 910 Poryazova R, Huber R, Khatami R, Werth E, Brugger P, Barath K, Baumann CR, Bassetti CL

- 911 (2015) Topographic sleep EEG changes in the acute and chronic stage of hemispheric
912 stroke. *J Sleep Res* 24:54-65.
- 913 Puentes-Mestril C, Aton SJ (2017) Linking Network Activity to Synaptic Plasticity during
914 Sleep: Hypotheses and Recent Data. *Front Neural Circuits* 11:1–18.
- 915 Robinson RG, Jorge RE, Moser DJ, Acion L, Solodkin A, Small SL, Fonzetti P, Hegel M,
916 Arndt S (2008) Escitalopram and problem-solving therapy for prevention of poststroke
917 depression: A randomized controlled trial. *JAMA - J Am Med Assoc* 299:2391–2400.
- 918 Rodriguez A V, Funk CM, Vyazovskiy V V, Nir Y, Tononi G, Cirelli C (2016) Why Does
919 Sleep Slow-Wave Activity Increase After Extended Wake? Assessing the Effects of
920 Increased Cortical Firing During Wake and Sleep. *J Neurosci* 36:12436–12447.
- 921 Rosanova M, Ulrich (2005) Pattern-Specific Associative Long-Term Potentiation Induced by
922 a Sleep Spindle-Related Spike Train. *J Neurosci* 25:9398–9405.
- 923 Sarasso S, Määttä S, Ferrarelli F, Poryazova R, Tononi G, Small SL (2014) Plastic Changes
924 Following Imitation-Based Speech and Language Therapy for Aphasia. *Neurorehabil*
925 *Neural Repair* 28:129–138.
- 926 Shah AM, Ishizaka S, Cheng MY, Wang EH, Bautista AR, Levy S, Smerin D, Sun G,
927 Steinberg GK (2017) Optogenetic neuronal stimulation of the lateral cerebellar nucleus
928 promotes persistent functional recovery after stroke. *Sci Rep* 7:46612.
- 929 Siccoli MM, Rölli-Baumeler N, Achermann P, Bassetti CL (2008) Correlation between sleep
930 and cognitive functions after hemispheric ischaemic stroke. *Eur J Neurol* 15:565–572.
- 931 Silasi G, Murphy TH (2014) Stroke and the Connectome: How Connectivity Guides
932 Therapeutic Intervention. *Neuron* 83: 1354-1368.
- 933 Small DL, Morley P, Buchan AM (1999) Biology of ischemic cerebral cell death. *Prog*
934 *Cardiovasc Dis* 42:185–207.
- 935 Steriade M, Nuñez A, Amzica F (1993) A novel slow(<1 Hz) oscillation of

- 936 neocortical neurons in vivo: depolarizing and hyperpolarizing components. *J Neurosci*
 937 13:3252–3265.
- 938 Steriade M, Timofeev I, Grenier F (2001) Natural waking and sleep states: a view from inside
 939 neocortical neurons. *J Neurophysiol* 85:1969–1985.
- 940 Stroh A, Adelsberger H, Groh A, Rühlmann C, Fischer S, Schierloh A, Deisseroth K,
 941 Konnerth A (2013) Making Waves: Initiation and Propagation of Corticothalamic Ca²⁺
 942 Waves In Vivo. *Neuron* 77:1136–1150.
- 943 Sun Y, Cheng X, Wang H, Mu X, Liang Y, Luo YJ, Qu H, Zhao C (2017) DL-3-n-
 944 butylphthalide promotes neuroplasticity and motor recovery in stroke rats. *Behav Brain*
 945 *Res* 329:67–74.
- 946 Talelli P, Wallace A, Dileone M, Hoad D, Cheeran B, Oliver R, VandenBos M, Hammerbeck
 947 U, Barratt K, Gillini C, Musumeci G, Boudrias M-H, Cloud GC, Ball J, Marsden JF,
 948 Ward NS, Di Lazzaro V, Greenwood RG, Rothwell JC (2012) Theta Burst Stimulation
 949 in the Rehabilitation of the Upper Limb. *Neurorehabil Neural Repair* 26:976–987.
- 950 Tennant KA, Taylor SL, White ER, Brown CE (2017) Optogenetic rewiring of
 951 thalamocortical circuits to restore function in the stroke injured brain. *Nat Commun*
 952 8:15879.
- 953 Timofeev I, Chauvette S (2017) Sleep slow oscillation and plasticity. *Curr Opin Neurobiol*
 954 44:116–126.
- 955 Tononi G, Cirelli C (2006) Sleep function and synaptic homeostasis. *Sleep Med Rev* 10:49–
 956 62.
- 957 Tononi G, Cirelli C (2014) Neuron Perspective Sleep and the Price of Plasticity: From
 958 Synaptic and Cellular Homeostasis to Memory Consolidation and Integration. *Neuron*
 959 81:12–34.
- 960 Tononi G, Cirelli C (2016) Sleep and Synaptic Down-Selection. In: *European Journal of*

- Neuroscience, pp 99–106.
- van Meer MPA, Otte WM, van der Marel K, Nijboer CH, Kavelaars A, van der Sprenkel JWB, Viergever MA, Dijkhuizen RM (2012) Extent of Bilateral Neuronal Network Reorganization and Functional Recovery in Relation to Stroke Severity. *J Neurosci* 32:4495–4507.
- Vock J, Achermann P, Bischof M, Milanova M, Müller C, Nirkko A, Roth C, Bassetti CL (2002) Evolution of sleep and sleep EEG after hemispheric stroke. *J Sleep Res* 11:331–338.
- Vyazovskiy V V, Faraguna U, Cirelli C, Tononi G (2009) Triggering slow waves during NREM sleep in the rat by intracortical electrical stimulation: effects of sleep/wake history and background activity. *J Neurophysiol* 101:1921–1931.
- Vyazovskiy V V., Olcese U, Hanlon EC, Nir Y, Cirelli C, Tononi G (2011) Local sleep in awake rats. *Nature* 472:443–447.
- Vyazovskiy V V., Olcese U, Lazimy YM, Faraguna U, Esser SK, Williams JC, Cirelli C, Tononi G (2009) Cortical Firing and Sleep Homeostasis. *Neuron* 63:865–878.
- Xie L, Kang H, Xu Q, Chen MJ, Liao Y, Thiyagarajan M, O'Donnell J, Christensen DJ, Nicholson C, Iliff JJ, Takano T, Deane R, Nedergaard M (2013) Sleep drives metabolite clearance from the adult brain. *Science* (80-) 342:373–377.
- Yang G, Lai C, Cichon J, Ma L, Li W, Gan W-B (2014) Sleep promotes branch-specific formation of dendritic spines after learning. *Science* (80-) 344:1173–1178.
- Yokoyama E, Nagata K, Hirata Y, Satoh Y, Watahiki Y, Yuya H (1996) Correlation of EEG activities between slow-wave sleep and wakefulness in patients with supra-tentorial stroke. *Brain Topogr* 8:269–273.
- Yoon KJ, Oh B-M, Kim D-Y (2012) Functional improvement and neuroplastic effects of anodal transcranial direct current stimulation (tDCS) delivered 1 day vs. 1 week after

- 986 cerebral ischemia in rats. *Brain Res* 1452:61–72.
- 987 Xu W, De Carvalho F, Jackson A (2019) Sequential neural activity in primary motor cortex
988 during sleep. *J Neurosci* 39:3698–3712.
- 989 Zhang X, Mei Y, Liu C, Yu S (2007) Effect of transcranial magnetic stimulation on the
990 expression of c-Fos and brain-derived neurotrophic factor of the cerebral cortex in rats
991 with cerebral infarct. *J Huazhong Univ Sci Technol* 27:415–418.
- 992 Zucca S, D’Urso G, Pasquale V, Vecchia D, Pica G, Bovetti S, Moretti C, Varani S, Molano-
993 Mazón M, Chiappalone M, Panzeri S, Fellin T (2017) An inhibitory gate for state
994 transition in cortex. *Elife* 6:1–31.
- 995

FIGURE LEGENDS

Figure 1. Stroke alters sleep architecture. (A) Schematic of the Circle of Willis (CW) with highlighted common carotid artery (CCA), internal carotid artery (ICA), middle cerebral artery (MCA) involved in MCAo procedure and filament placement. (B) Coronal sections (40 μ m) of a representative mouse 15 days after MCAo. Nissl staining. (C) Schematic representation of EEG and EMG electrodes placements relative to stroke. 24 h recordings of animals' sleep-wake cycles were performed before stroke (Baseline) and again at post-stroke day 1, 3, 5 and 10 in Stroke (n = 11) and Sham (n = 9) animals. (D) Percentage changes of wakefulness, NREM sleep (E) and REM sleep (F) total durations from each animal's baseline values. (G) Comparison between bout durations of wakefulness, NREM sleep (H) and REM sleep (I). (J) Ratio between NREM continuous episodes and transitions to wake. (K) Total number of microarousals in 24 h recordings. (L) Percentage of epochs spent in wake or sleep states for Stroke (blue table) and Sham (grey table) groups, respectively. Linear mixed model of 8 matrices: Wake duration changes; NREM duration changes; REM duration changes; Wake bout duration; NREM bout duration; REM bout duration; NREM stability; Microarousals. Data are represented as means \pm s.e.m.; asterisks indicate significance *p < 0.0063.

Figure 2. Stroke alters SW profile. (A) Automatic detection of single slow waves (SW) from local field potential (LFP) recordings in ipsilateral primary somatosensory forelimb cortex (iS1FL), ipsilateral primary motor cortex (iM1), contralateral M1 (cM1), contralateral S1FL (cS1FL) and EEG traces from ipsilateral (iEEG) and contralateral (cEEG) hemispheres. Representative traces in black and detected SW in colours (top). Magnification of one episode of NREM sleep and detected SW (bottom). (B) Schematic of tetrodes and EEG/EMG electrode implantation. (C) Representative average SW from 24 h baseline EEG recording.

1022 (D) Unit activity heat map of neurons recorded during detected SW; the graph shows
 1023 neuronal activity suppression corresponding to the silent SW DOWN state (top). Average
 1024 firing rate of single units recorded during the detected SW (bottom). (E) Schematic of EEG
 1025 electrodes position. (F) SW peak to peak amplitude prior to (Baseline) and following MCAo
 1026 or sham surgery (post stroke day 1, 3, 5 and 10). (G) SW positive slope. (H) SW negative
 1027 slope. (I) Number of single SW detected. (J) SW duration. Stroke $n = 11$, Sham $n = 9$; two-
 1028 way ANOVA, followed by Bonferroni post-hoc test. Data are represented as means \pm s.e.m.
 1029 Asterisks indicate significance $*p < 0.05$.

1030

1031 **Figure 3.** Optogenetic induction of SW-like bistable oscillations. (A) Scheme of a coronal
 1032 brain section with AAV injection site (left), AAV structure (top) and optrode/EEG/EMG
 1033 implantation representation (right). (B) Opsin distribution within the peri-infarct ipsilateral
 1034 primary somatosensory forelimb cortex (iS1FL) following AAV injection of CaMKII-ChR2-
 1035 EYFP. (C) Local field potential (LFP) traces, single unit activity and correspondent raster
 1036 plot and mean spike rate upon optogenetic stimulation during wakefulness (left), NREM
 1037 sleep (middle) and REM sleep (right) from one representative stimulation session. (D)
 1038 Average ipsilateral (iEEG) and contralateral EEG (cEEG) traces response to activation
 1039 (ChR2) of pyramidal neurons with 5 ms of single laser light pulses (473 nm). (E) Comparison
 1040 between spontaneous and optogenetically-evoked SW (SW^{opto}) duration (left), negative
 1041 amplitude (middle) and slope (right) during NREM sleep for ChR2 stimulated animals;
 1042 Wilcoxon rank sum test, statistically significant if $p < 0.05$. (F) ArchT distribution within
 1043 iS1FL. (G) Representative EEG/EMG traces upon silencing of pyramidal neurons with 200
 1044 ms of single laser light pulses (532 nm) during NREM sleep. (H) Average iEEG and cEEG
 1045 responses to ArchT stimulation. (I) Comparison between SW^{opto} duration (left), negative
 1046 amplitude (middle) and slope (right) during NREM sleep for ArchT stimulated animals;

1047 Wilcoxon rank sum test, statistically significant if $p < 0.05$. (J) mCherry (control) expression
 1048 in iS1FL; representative EEG/EMG responses during 5ms light pulse stimulation (top) and
 1049 average EEGs (bottom). (L) Representative EEG/EMG traces response to 200ms pulse
 1050 stimulation in one mCherry transfected mouse (top) and its average EEGs response.

1051

1052 **Figure 4.** Optogenetic screening for slow waves induction in the peri-infarct zone. (A)
 1053 Coronal section indicating the AAV injection site (left primary somatosensory forelimb
 1054 cortex, S1FL) (top) and schematic of EEG/EMG/optic fiber/tetrodes implantation (bottom).
 1055 (B) LFP recordings from S1FL upon laser light stimulation (500 ms, 5 Hz and 200 ms) of
 1056 inhibitory (top) or pyramidal neurons (bottom) respectively.

1057

1058 **Figure 5.** SW^{opto} oscillations travel across hemispheres. (A) Local field potential (LFP)
 1059 traces, multi-unit activity from tetrodes placed in ipsilateral primary somatosensory forelimb
 1060 cortex (iS1FL), contralateral S1FL (cS1FL), ipsilateral primary motor cortex (iM1) and
 1061 contralateral M1 (cM1) and EEG/EMG traces recorded during one stimulating session
 1062 showing the travelling characteristic of the evoked waves (SW^{opto}). (B) Raster plots
 1063 corresponding to one single light pulse stimulation event during wakefulness, NREM and
 1064 REM sleep as well as relative mean spike rate for iS1FL, cS1FL, cM1 respectively. No unit
 1065 was found for iM1. (C) Average LFP traces during the stimulation events for the four
 1066 recorded cortical areas respectively.

1067

1068 **Figure 6.** SW^{opto} defines a critical window of intervention for stroke recovery. (A) When the
 1069 stimulation protocol started at post-stroke day 1, $ChR2^{stroke}$ animals in particular showed
 1070 lower survival percentage. (B) When the stimulation instead began at post-stroke day 5,

1071 ChR2^{stroke} animal showed an improvement in survival percentage. Asterisks indicate
1072 significance * $p < 0.05$.

1073

1074 **Figure 7.** SW^{opto} during sleep improves functional recovery after stroke. (A) Schematics of
1075 optic fiber/EEG/EMG implantation with opsin expression site. (B) Experimental timeline. (C)
1076 Average number of single light pulses within sleep stages during the stimulation sessions of
1077 ArchT^{stroke}, ChR2^{stroke}, mCherry^{stroke}, mCherry^{sham} and ChR2^{stroke_wake} respectively. (D)
1078 Stimulated animals showed better performances in the ladder walking rig test compared to
1079 mCherry-control animals (Naive $n = 8$, mCherry^{sham} $n = 8$, ArchT^{stroke} $n = 4$, ChR2^{stroke} $n = 7$,
1080 mCherry^{stroke} $n = 6$). Induction of slow waves mainly during wakefulness (ChR2^{stroke_wake} $n =$
1081 6) did not result in faster improvement of performance compared to ChR2^{stroke} stimulated
1082 during NREM sleep. Linear mixed model. (E) Percentage of improvement from post-stroke
1083 day 4 to post-stroke day 15 for ChR2^{stroke} groups and ArchT^{stroke} compared to mCherry^{stroke}
1084 control (one-way ANOVA). (F) Similar results was observed for performances in the balance
1085 test (Naive $n = 8$, mCherry^{sham} $n = 6$, ArchT^{stroke} $n = 7$, ChR2^{stroke} $n = 7$, mCherry^{stroke} $n = 7$,
1086 ChR2^{stroke_wake} $n = 6$). (G) Balance beam percentage of improvement from post-stroke day 4
1087 to post-stroke day 15 for ChR2^{stroke} groups and ArchT^{stroke} compared to mCherry^{stroke} control
1088 (one-way ANOVA). (H) Tight rope test and corner test (I) did not show differences between
1089 stimulated and control groups (Naive $n = 8$, mCherry^{sham} $n = 6$, ArchT^{stroke} $n = 7$, ChR2^{stroke} n
1090 $= 6$, mCherry^{stroke} $n = 8$, ChR2^{stroke_wake} $n = 6$). Asterisks indicate significances * $p < 0.05$.

1091

1092 **Figure 8.** SW^{opto} increases axonal sprouting during stroke recovery. (A) Scheme of a brain
1093 coronal section 15 days after stroke (end point of experiment) representing tissue atrophy
1094 corresponding to the stroke area. Confocal micrograph of iS1FL with 3D reconstruction of
1095 pre- and post-synaptic markers contact (right). Blue: DAPI staining; red: Vglut1 pre-synaptic

1096 marker; aquamarine: PSD-95 post-synaptic marker. (B) Comparison of Vglut1 puncta
 1097 density between iS1FL and cS1FL cortical areas (mCherry^{stroke} n = 4, ChR2^{stroke} n = 4,
 1098 ArchT^{stroke} n = 4, mCherry^{sham} n = 4) in ipsilateral (F (3, 19) = 10.49, p = 0.0003) and
 1099 contralateral layers II (F (3, 19) = 1.069, p = 0.385), as well as in ipsilateral (F (3, 18) =
 1100 16.02, p < 0.0001) and contralateral layers V (F (3, 21) = 11.05, p = 0.0001) (C). (D) Vglut1
 1101 puncta volume distribution in iS1FL layer II (F (2, 1630) = 34.85, p < 0.0001) and layer V
 1102 (E) summarized in bar graph (F (2, 1617) = 155, p < 0.0001). (F) Comparison of PSD-95
 1103 puncta density in ipsilateral (F (3, 23) = 8.609, p = 0.0005) and contralateral (F (3, 21) =
 1104 1.105, p = 0.369) layers II, as well as in ipsilateral (F (3, 24) = 1.095, p = 0.370) and
 1105 contralateral (F (3, 24) = 2.498, p = 0.083) layers V (G). (H) PSD-95 puncta volume
 1106 distribution in iS1FL layer II summarized in bar graph (F (2, 2070) = 9.164, p = 0.0001); (I)
 1107 iS1FL layer V (F (2, 2111) = 75.13, p < 0.0001). One way-ANOVA. Data are represented as
 1108 means \pm s.e.m. Asterisks indicate significance *p < 0.05. n.s. = not significant.

Figure 1

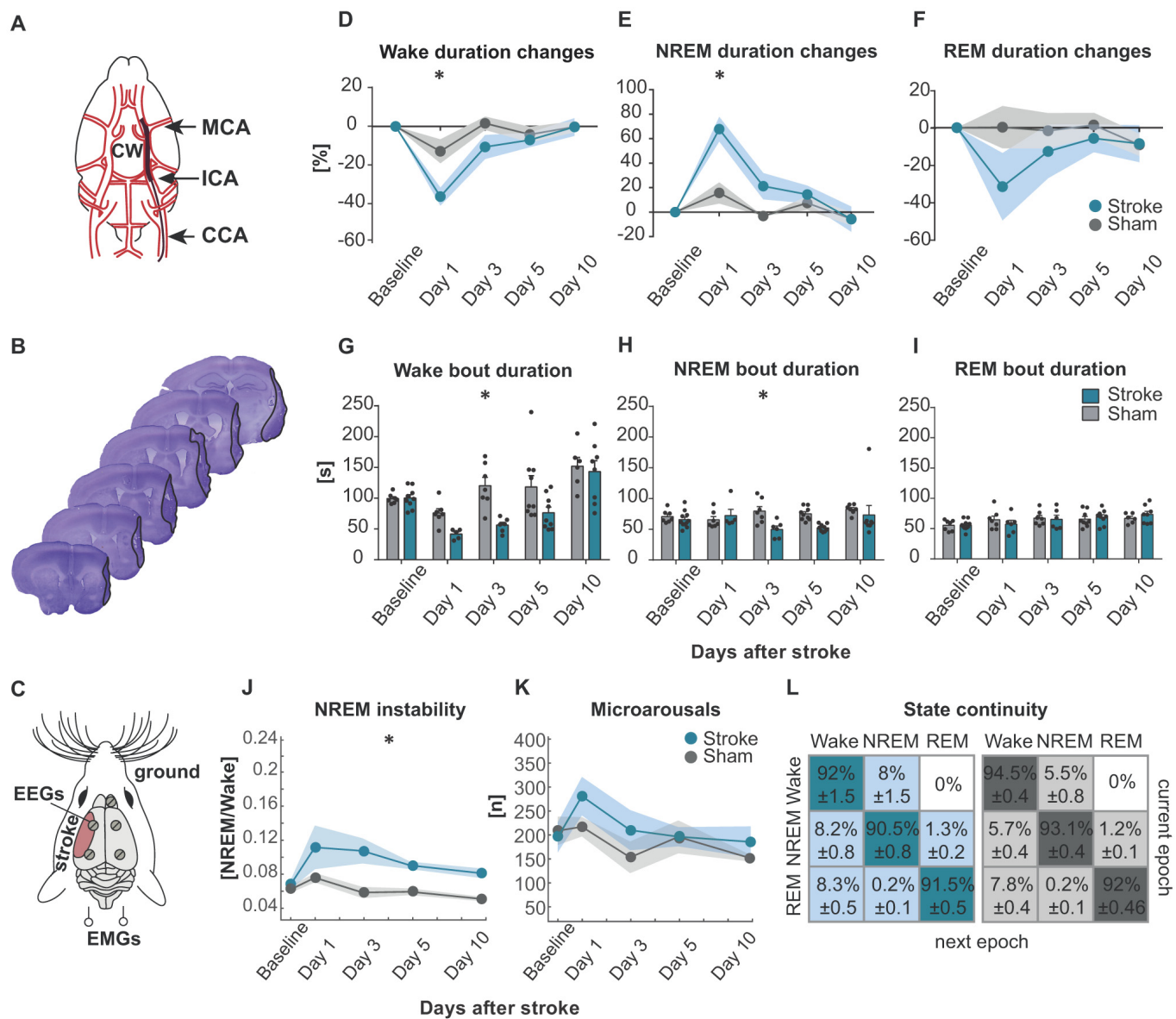


Figure 2

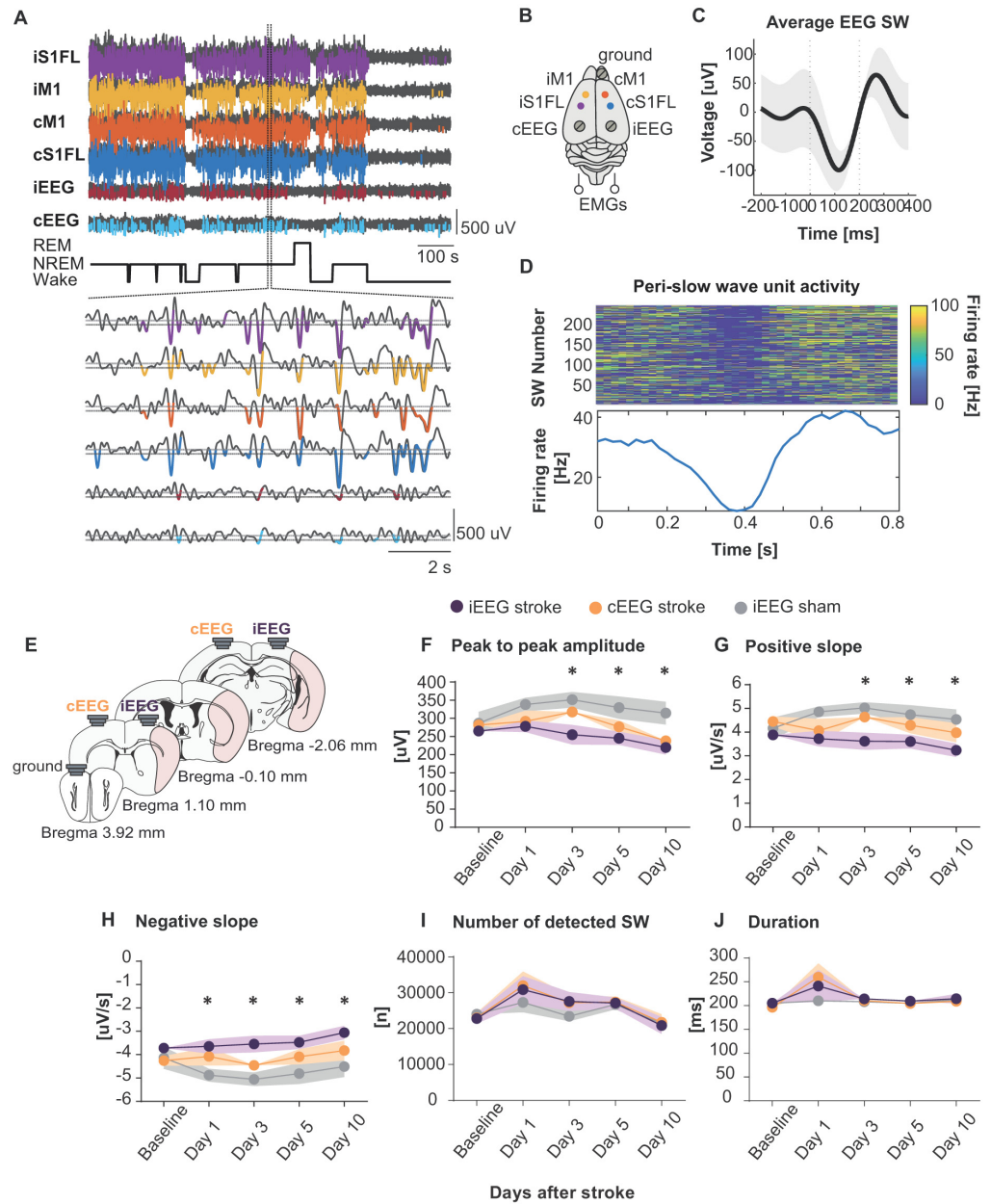
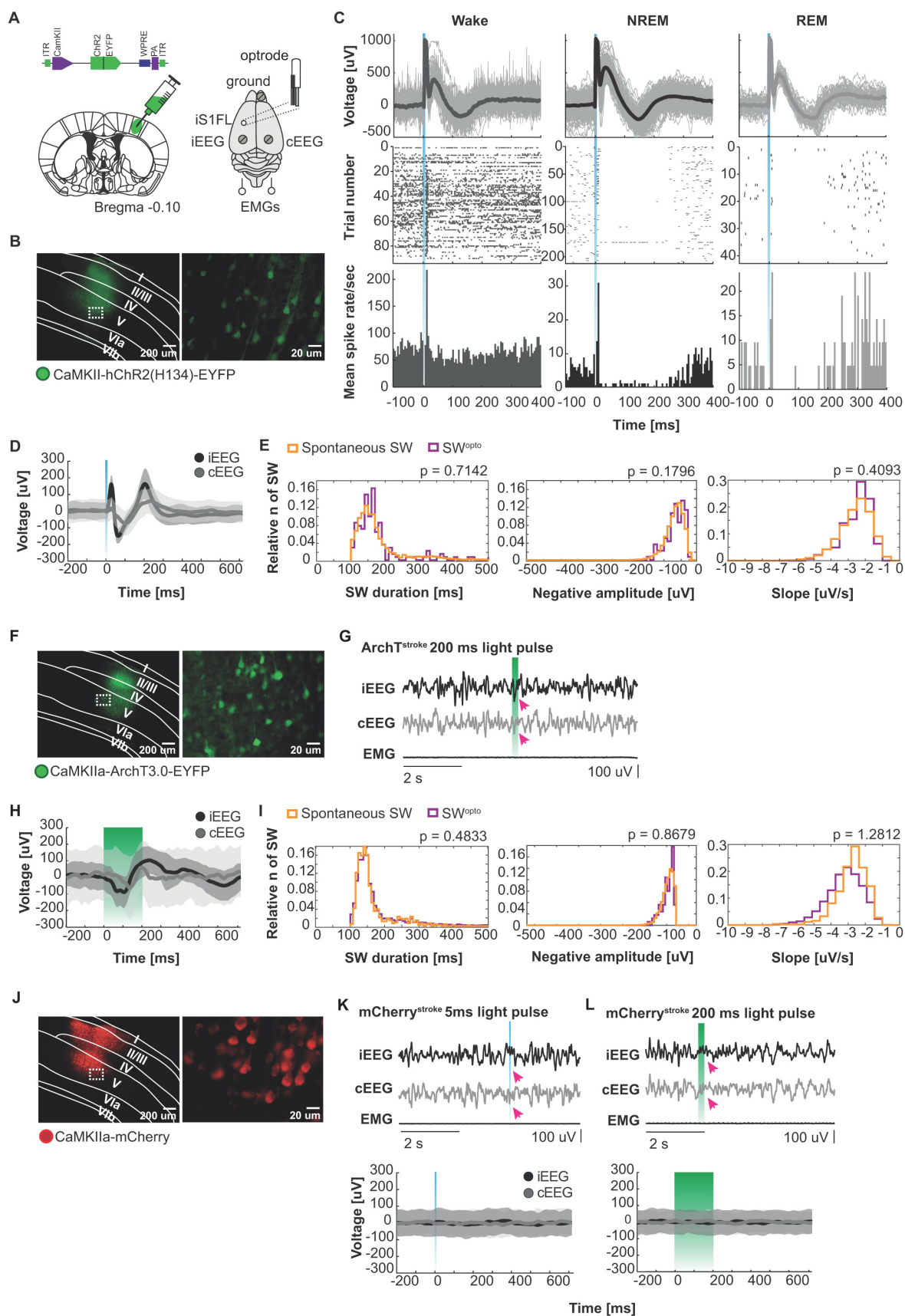


Figure 3



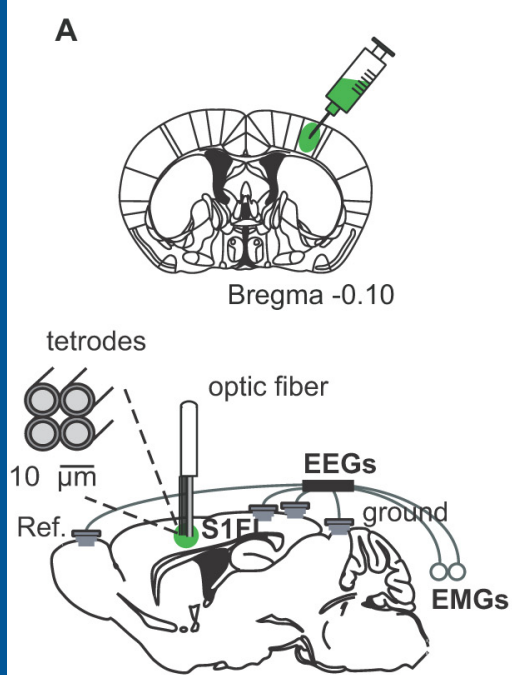


Figure 4

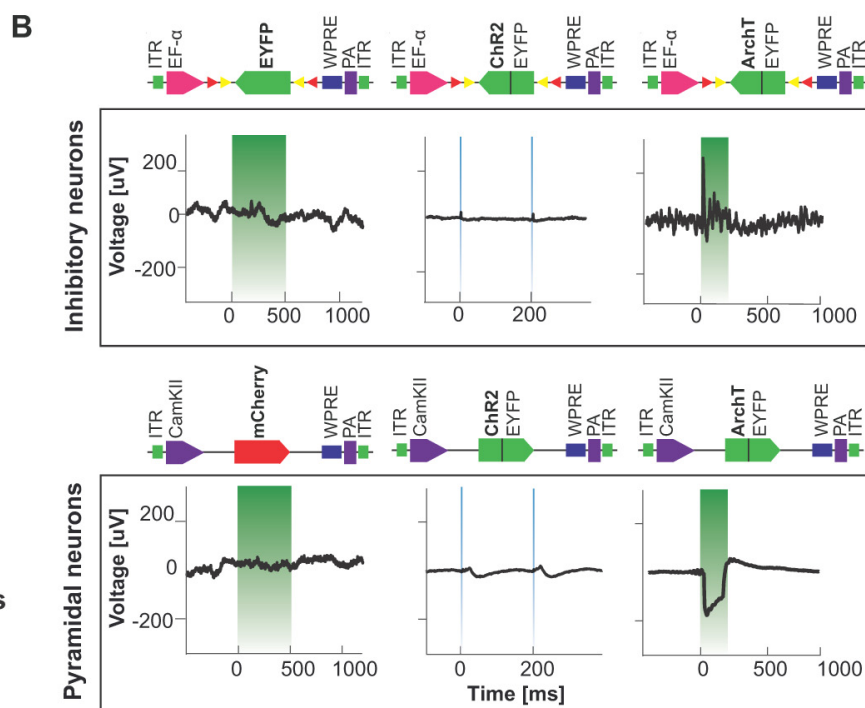


Figure 5

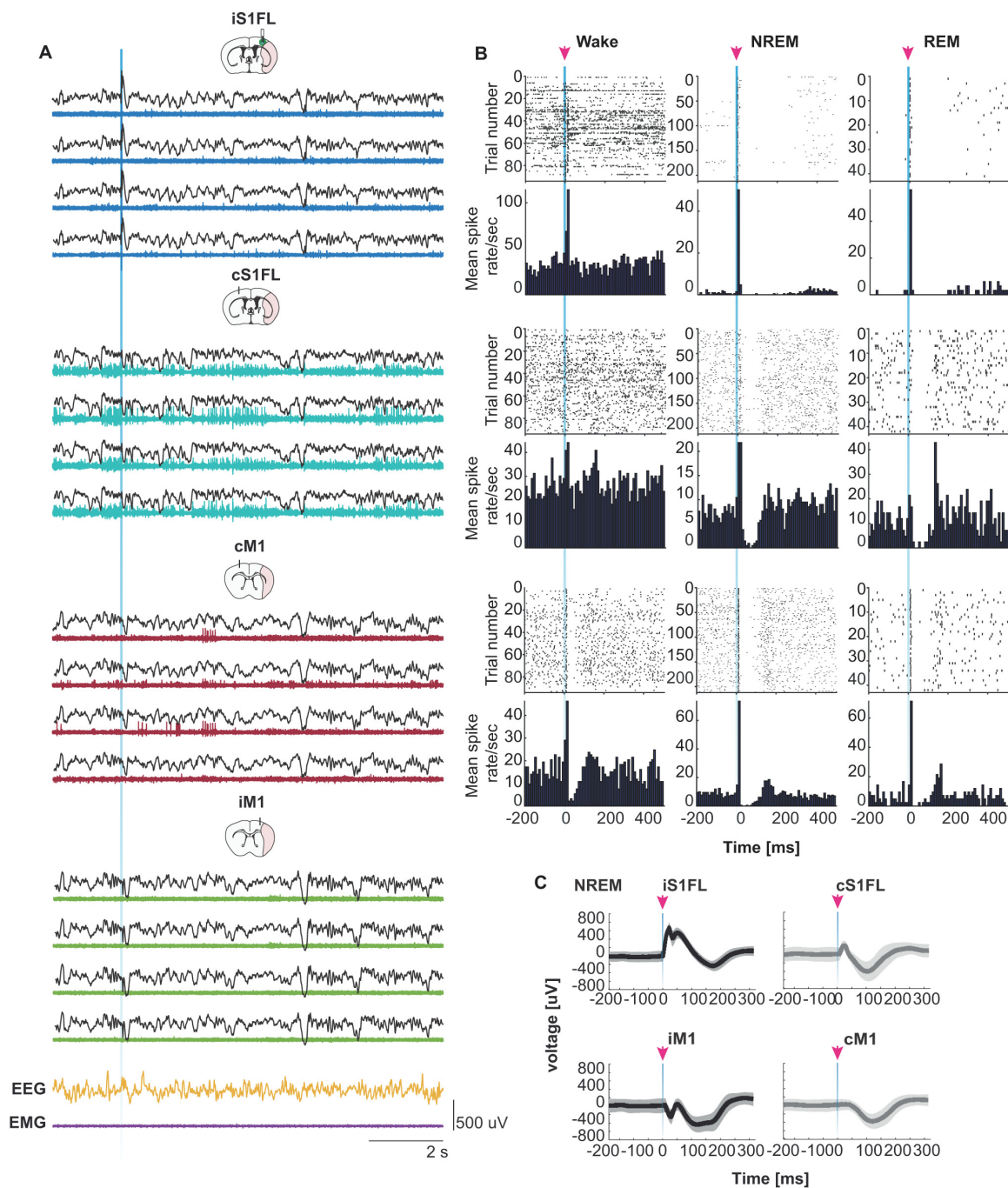


Figure 6

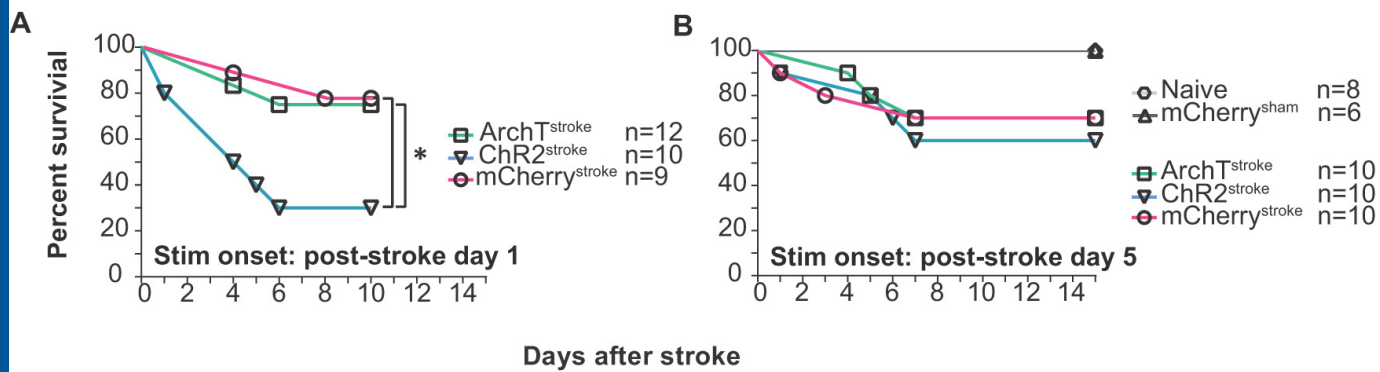


Figure 7

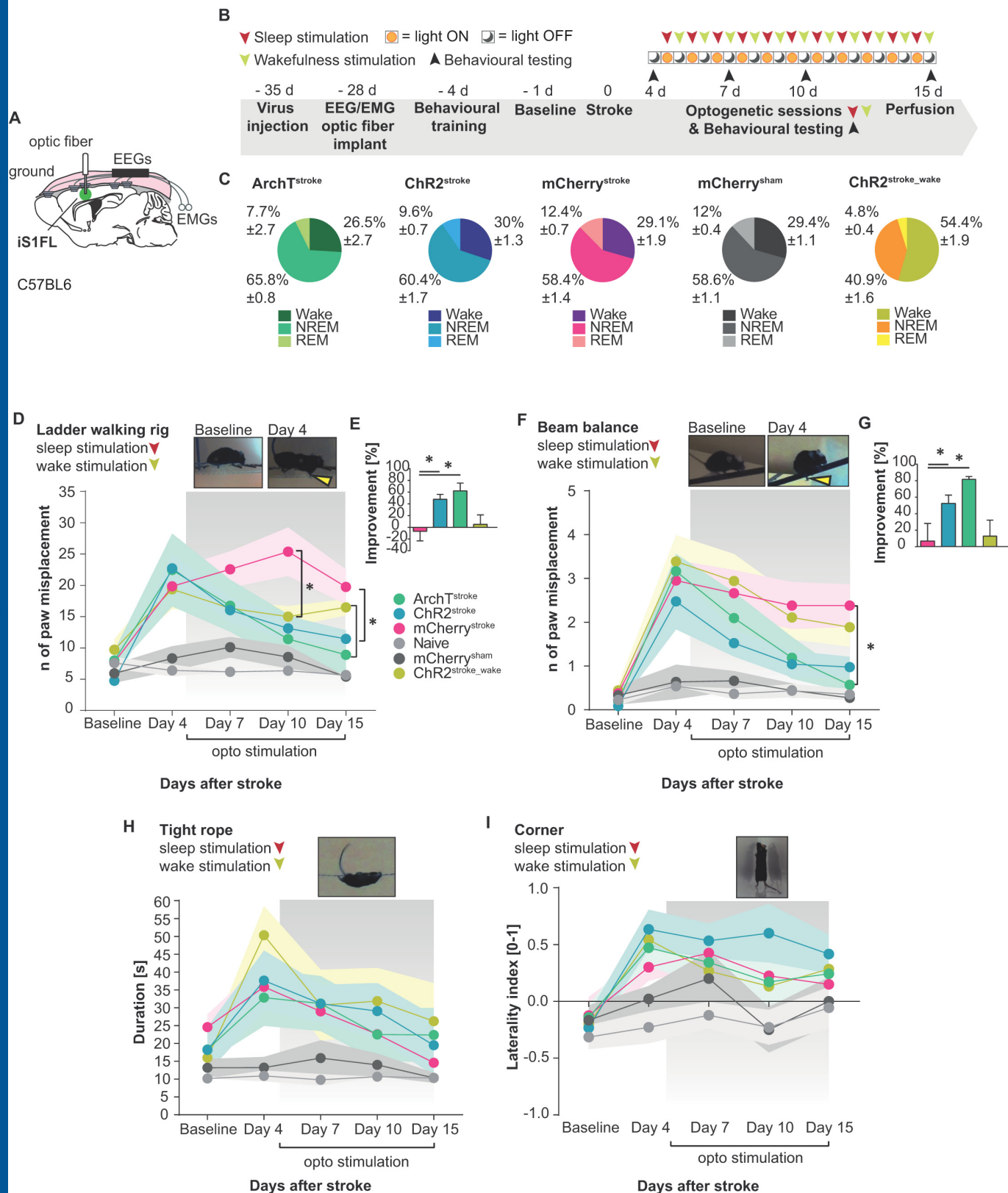


Figure 8

